2009-07-14

A Methodology for Designing Product Components with Built-in Barriers to Reverse Engineering

Stephen P. Harston
Brigham Young University - Provo

A METHODOLOGY FOR DESIGNING PRODUCT COMPONENTS WITH BUILT-IN BARRIERS TO REVERSE ENGINEERING

by

Stephen P. Harston

A thesis submitted to the faculty of

Brigham Young University

in partial fulfillment of the requirements for the degree of

Master of Science

Department of Mechanical Engineering

Brigham Young University

August 2009

BRIGHAM YOUNG UNIVERSITY

GRADUATE COMMITTEE APPROVAL

of a thesis submitted by

Stephen P. Harston

This thesis has been read by each member of the following graduate committee and by majority vote has been found to be satisfactory.

Date	Christopher A. Mattson, Chair
Date	Brent L. Adams
Date	Brian D. Jensen

BRIGHAM YOUNG UNIVERSITY

As chair of the candidate's graduate committee, I have read the thesis of Stephen P. Harston in its final form and have found that (1) its format, citations, and bibliographical style are consistent and acceptable and fulfill university and department style requirements; (2) its illustrative materials including figures, tables, and charts are in place; and (3) the final manuscript is satisfactory to the graduate committee and is ready for submission to the university library.

Date

Christopher A. Mattson
Chair, Graduate Committee

Accepted for the Department

Larry L. Howell
Graduate Coordinator

Accepted for the College

Alan R. Parkinson
Dean, Ira A. Fulton College of
Engineering and Technology

ABSTRACT

A METHODOLOGY FOR DESIGNING PRODUCT COMPONENTS

WITH BUILT-IN BARRIERS TO REVERSE ENGINEERING

Stephen P. Harston

Department of Mechanical Engineering

Master of Science

Reverse engineering, defined as extracting information about a product from the product itself, is a common industry practice for gaining insight into innovative products. Both the original designer and those reverse engineering the original design can benefit from estimating the time and barrier to reverse engineer a product. This thesis presents a set of metrics and parameters that can be used to calculate the barrier to reverse engineer any product as well as the time required to do so. To the original designer, these numerical representations of the barrier and time can be used to strategically identify and improve product characteristics so as to increase the difficulty and time to reverse engineer them. One method for increasing the time and barrier to reverse engineer a product – presented in this thesis – is to treat material microstructures (crystallographic grain size, orientation, and distribution) as continuous design variables that can be manipulated to identify unusual material properties and to design devices with unexpected mechanical performance. A practical approach, carefully tied to proven manufacturing strategies, is used to tailor material microstructures by strategically orienting and laminating thin anisotropic metallic sheets. This approach, coupled with numerical optimization, manipulates material microstructures

to obtain desired material properties at designer-specified locations (heterogeneously) or across the entire part (homogeneously). As the metrics and parameters characterizing the reverse engineering time and barrier are also quantitative in nature, they can also be used in conjunction with numerical optimization techniques, thereby enabling products to be developed with a maximum reverse engineering barrier and time – at a minimum development cost. On the other hand, these quantitative measures enable competitors who reverse engineer original designs to focus their efforts on products that will result in the greatest return on investment. While many products were analyzed in an empirical study demonstrating that the characterization of the time to reverse engineer a product has an average error of 12.2%, we present the results of three different products. Two additional examples are also presented showing how microstructure manipulation leads to product hardware with unexpected mechanical performance effectively increasing reverse engineering time and barrier.

ACKNOWLEDGMENTS

I would like to acknowledge and express appreciation for all those who have helped and inspired me throughout this research.

I especially would like to thank my advisor, mentor, and friend, Dr. Christopher A. Mattson. His innate ability to inspire and motivate one to perform above and beyond their natural capabilities is evident in the level of success we have had in the research. Because of his guidance, this research experience has been excellent as he has molded me into being a better person in all aspects of my life.

I am also grateful for Dr. Brent L. Adams and the help and inspiration he has given me. His patience and ability to teach difficult subjects is a gift and I am grateful for the extra patience that was required to teach me. Thanks to Dr. Brian D. Jensen for his advice and help with the design and analysis of bistable mechanisms – a fundamental aspect of the research.

I would also like to acknowledge the National Science Foundation and the funding that was received from them under grant CMMI-0800904 for Christopher A. Mattson and Brent L. Adams.

Importantly, I want to express my undying gratitude to my amazing wife who was so willing and supportive during the many long days and nights that were devoted to research. Above all, I acknowledge and am grateful for the Divine guidance that has been a constant blessing throughout all aspects of the research and my life.

Table of Contents

List of Tables

List of Figures

Nomenclature

B	Barrier to extract information about a product from the product itself
$\overline{D}$	Macroscopic strain rate
D_0	First component of strain rate tensor
D_k^N	Normal direction of the k-th lamina, also an axis for the lamina reference frame
D_k^R	Rolling direction of the k-th lamina, also an axis for the lamina reference frame
D_k^T	Transverse direction of the k-th lamina, also an axis for the lamina reference frame
$\overline{d}$	Average grain size
Δg	Volume of discretized bins in Fundamental Zone
E	Young's modulus
$E_m(wxyz)$	Fourier coefficients representing Young's modulus in the $wxyz$ direction for the m-th bin of the Fundamental Zone
F	Estimated rate at which information is extracted from a product
F_m	Fourier coefficients of crystal volume fraction in the m-th bin of the Fundamental Zone
G	Shear modulus
g	Euler angles from Sample to Crystal reference frames
g_{wx}	Orientation matrix of Euler angles from Sample to Crystal reference frames
$\dot{\gamma}$	Shear rate
$\dot{\gamma}_0$	Reference shear rate
K	Estimated or actual information contained by a product
L	Distance between straight, parallel lines used to determine average grain size
λ	The contraction ratio for the strain tensor
M	Material class, (e.g., nickel, copper)
M_0	Selected alloy from material class
N	Number of laminae to be used in layer-by-layer creation of material

n	Inverse rate sensitivity parameter
n_c	Number of columns in the binned Fundamental Zone
n_h	Number of layers in the binned Fundamental Zone
n_r	Number of rows in the binned Fundamental Zone
ν	Poisson's ratio
P	Estimated power exerted to extract information contained by a product
$\phi_{1,i}$	Lamination orientation for the i-th layer
S	A measure of a product's ability to contain information
S_{11}	Material property constant obtained from literature for selected material class
S_{12}	Material property constant obtained from literature for selected material class
S_{44}	Material property constant obtained from literature for selected material class
$\overline{S}(wxyz)$	Sample compliance (average crystal compliance)
s	Slip systems. Comprised of slip plane normals, $\{111\}$, and slip directions $< 110 >$
σ'_{ij}	Deviatoric stress
σ_y	Yield strength
T	Estimated time to extract information K
t	Reference time frame for reverse engineering a product
τ	Reference time frame when all parameters are known
τ_0	Lattice friction stress
τ^*	Reference shear stress
Y_m	Fourier coefficients representing yield strength physics

Subscripts, superscripts, and other indicators

$[\,]^*$	indicates total measure or effective property
$[\,](t)$	indicates $[\,]$ is a function of time, in the t domain
$[\,](\tau)$	indicates $[\,]$ is a function of time, in the τ domain
$[\,]_0$	indicates $[\,]$ is evaluated at time t or τ equal to zero
$[\,]_p$	indicates $[\,]$ is in the part reference frame
$[\,]_c$	indicates $[\,]$ is in the crystal reference frame
$[\,]_l$	indicates $[\,]$ is in the lamina reference frame
$[\,]_t$	indicates $[\,]$ is the target value

Chapter 1

Introduction

The introduction of innovative products into the marketplace is often accompanied by an interesting engineering and design dichotomy; on the one hand, the original designer is intent on maintaining his/her competitive advantage, gained through innovation, by offering the product to the masses without easily disclosing its enabling technology [1]. On the other hand, however, the competitor is determined to reverse engineer the innovative product so as to uncover the enabling technology and potentially earn a portion of the market by capitalizing on it [2, 3]. For clarity of scope, we provide three important definitions in the context of this thesis:

Reverse Engineering is the process of extracting information about a product from the product itself.

Time to Reverse Engineer is the total required man-time to reverse engineer a product without consideration to parallel activities.

Barrier to Reverse Engineering is anything that impedes reverse engineering.

There are numerous cases where a company has spent months engineering and developing a product only to have a competing company create a reverse engineered version within a few weeks of it being publicly available [4]. Interestingly, there are few laws to prevent the reverse engineering of hardware [5]. Current laws state that reverse engineering is an acceptable method of obtaining trade secrets as long as the product acquisition was done legitimately [5]. These laws are rationalized, by many, since the time and effort required to reverse engineer a product is often viewed as substantial enough to allow the original designer to maintain a large market share [5]. If the justification of the current laws

was true then reverse engineering would not be a common issue. Since reverse engineered products are taking a substantial part of the market share [6] it is desirable for developing companies to maximize the time and effort required to reverse engineer their products.

Almost exclusively, when a product is reverse engineered, it comes at some cost to the original company. Often the cost is monetary, one example being the Chevy Spark (a compact car sold in Asia). Soon after the release of the Chevy Spark it was being reproduced nearly identically as the Chery QQ by the Chinese automotive company Chery. The Chery QQ currently outsells the Chevy Spark nearly five to one [6]. Other times, market share lost due to a reverse engineered product is negligible when compared to the national security lost when Armed Forces equipment is captured and reverse engineered. The B-29 Superfortress is an American bomber that was captured by Russia during World War II. Only two years after the capture of the B-29, Russia was performing their own bombing raids with the first of 847 Tu-4's, an identical copy of the American B-29, to be built by Russia. The Tu-4 was engineered so precisely that it even had the same problems as the B-29 such as notoriously unreliable engines [7].

Although seen from different perspectives, the notion of *barriers to reverse engineering* is critical for both the original designer and the competitor who performs reverse engineering activities. Ideally, to the original designer, all efforts are made to increase the barrier and time required to reverse engineer his/her design. To those reverse engineering the original designs, minimal time and barrier is desired so as to enter the market before it is saturated. In either case, these designers could benefit from general metrics and parameters for quantifying the time and barrier to reverse engineer a product [8, 9].

The purpose of this thesis is to develop a design methodology that increases the time and barrier to reverse engineer products. These barriers to reverse engineering include, for example, critical complex surfaces that are difficult to recreate, localized heat treating that creates difficult-to-discover heterogeneous material characteristics, and hidden in situ sensors that monitor performance. In order to obtain and design for these barriers, we must:

1. Be able to measure the time and barrier to reverse engineering and know what it affects.

2. Determine the effects of manufacturing on the time and barrier enabling one to determine manufacturing recipes that maximizes the time and barrier.

3. Verify and demonstrate that the barrier to reverse engineering can be maximized.

Chapter 2

Literature Survey

Reverse engineering has been defined in a variety of similar, yet unique, ways by the disciplines that have approached the topic in the literature [2,10,11]. Among the various disciplines that have addressed the topic of reverse engineering the following three areas are predominant; (i) reverse engineering of software [10, 12–15] (ii) reverse engineering of hardware [2,3,8,16,17], and (iii) reverse engineering of biological systems [11,18–20]. The reverse engineering of software is pervasive in the literature and is of particular interest as it relates to reverse engineering because software is being delivered to end-users with more mobile code in architecture-independent formats – thereby facilitating the reproduction of original code with less effort. Strategies to prevent reverse engineering of software include tamper proofing, obfuscation, and watermarking [21].

The reverse engineering of hardware is generally addressed in the literature from within three areas of research; (i) performance benchmarking [2,3,17], which is the evaluation of competitive products in order to specify performance criteria and generate concepts for new products, (ii) geometric surface and shape recovery [22,23], which is the automated extraction of geometry from an existing product and the construction of 3D CAD models from the data, and (iii) empirical parameter estimation and surrogate model building by statistical sampling of hardware [24, 25], which is simply the estimation of performance measures through testing an existing product and fitting a mathematical model to the test data, thereby developing an approximate parametric model of the product's performance.

Ingle provides a basic four-stage methodology for the reverse engineering of hardware [2]. Of the four stages presented by Ingle, the first two stages are of particular interest in the context of this thesis; Stage 1 is the evaluation and verification of a product or sys-

tem, and Stage 2 is the documentation of the findings, usually in the form of technical data. As a note, Stage 3 is prototype verification, and Stage 4 is project implementation.

Finally, research in the reverse engineering of biological systems has gained more and more momentum as scientists and engineers seek to discover the building blocks of nature [18, 19] and successful ways in which natural systems accomplish complex tasks [20].

Although related and useful to the design and reverse engineering of software, hardware, and biological systems, the developments presented in this thesis focus on an articulated, yet unmet need in the literature – comparative metrics for barrier and time to reverse engineer a product or system. Various researchers have expressed the need to estimate the time and barrier to reverse engineer a product. The various perspectives in the literature range from those of the original designer [8, 16, 17], to those who reverse engineer, [2, 3, 9], to market analysts [8, 26, 27]. While these perspectives are insightful and suggest the need for quantitative measures, unfortunately none of them provide it.

Macmillan et al. [8], state that it is critical to estimate competitor's response lag (or time to reverse engineer and imitate a product) in order to understand the potential financial risks and profits. Pahl et al. [17] state that effective product planning includes understanding the life cycle of the proposed product as well as understanding competitor's products. Therefore, effective product planning and definition of product life cycle is likely to (i) consider the time required for competitors to conduct reverse engineering activities, *and* (ii) require a full understanding of competitive products through reverse engineering activities.

Shapiro [28] and Nelson and Winter [29] emphasize that the harder a product is to reverse engineer – dependent upon the competitor and their resources and skills available – the less incentive a competitor has to imitate the technology. On the other hand, there is little incentive for original designers to develop innovative products if competitors can imitate the products at a significantly reduced development cost with a larger return on investment [9].

While others have previously presented the idea of barriers to reverse engineering [16, 30, 31], we pursue the concept of barriers to reverse engineering further by devel-

oping relationships that define quantitative representations of the barrier and time to reverse engineer any product. We also explore techniques by which the reverse engineering barrier can be maximized. Specifically, we explore geometry and microscopic metallurgical material characteristics and their effects on the barrier to reverse engineering.

The optimization of macroscopic geometry, known in the literature as size [32], shape [33], and topology [34] optimization, is a powerful approach to identify hardware with desirable performance characteristics [35]. A different, yet equally powerful, approach is to manipulate microscopic metallurgical material characteristics to enhance material properties and achieve desirable hardware performance [36]. Individually, these two approaches have improved products and allowed for more advanced designs over those of the past [35, 36]. Through an integrated approach, however, macroscopic *and* microscopic features can be manipulated in a complementary way to identify hardware designs with desirable *and* unexpected mechanical performance thus resulting in a large barrier to reverse engineering.

While others have previously coupled material properties with geometry optimization [37, 38], we present a new method of tailoring the properties of metals by using thin laminations strategically oriented [39] and ultrasonically welded together [40]. We show how numerical optimization can be used to generate a complete materials design space [41–43] that envelops all possible property combinations for a given alloy. We also show that the proposed integration of optimization, manufacturing, and design methods can result in desired material properties that are consistently producible from a manufacturing perspective while simultaneously being nearly impossible to reproduce without knowing the precise manufacturing strategy. The proposed method can, therefore, be used to tailor new and practical materials for the design engineer's specific need with an increased barrier to reverse engineering.

In summary, there are two main needs expressed in the literature; (i) comparative metrics for the barrier and time to reverse engineer a product or system, and (ii) a design strategy that effectively seeks to maximize barriers to reverse engineering.

In this thesis, we demonstrate how these unmet needs are fulfilled by the methodologies presented herein. We start by discussing the fundamental relationships that enable

characterization of the reverse engineering time and barrier. These relationships originate from Ohm's law and enable us to estimate the time to reverse engineer a product with an average error of 12.2%. In Chapter 3 we present a brief overview of the pertinent relationships used from Ohm's law. The adaption of Ohm's law to product development is then presented in Chapter 4, followed by empirical validation of the developed relationships in Chapter 5. In Chapter 6 we review technologies and theories that enable one to obtain desired material properties from the framework presented in Chapter 7. Two case studies are presented in Chapter 8 demonstrating how the framework presented in Chapter 7 can be used to obtain desired material properties. The time and barrier to reverse engineer a homogeneous and a heterogeneous bistable switch are also calculated and discussed in Chapter 8. Concluding remarks are provided in Chapter 9.

Chapter 3

Technical Preliminaries

Ohm published the electrical relationship known as Ohm's law in 1827 [44]. Since then, it has been adapted and used to meaningfully characterize the behavior of many systems including fluid systems [45], mechanical systems [46], thermal systems [47], and electrical systems [48, 49].

Insightful discussions by Hartley [50] and Shannon [51] present *information* as a measurable quantity and support our notion that information extraction occurs in an exponential fashion. When the fundamental principles are analyzed as to why information extraction can be modeled as an exponential relationship, one discovers many similarities between the flow of information and the flow of electrons – thus leading to an adaptation of Ohm's law to model information extraction. The adaptation is rooted in the following: There exists a resistance to extracting information from a product much in the same way a resistor inhibits the flow of electrons. Also, products contain a quantity of information which is extracted during the reverse engineering process in a similar manner that capacitors discharge a quantity of stored electrons.

As a foundation for the ensuing developments, we consider the analysis of the simple resistor-capacitor circuit shown in Figure 3.1, and outline mathematical relationships that enable the evaluation of a circuit's resistance, R, capacitance, C, and the time, T, to drain an initially charged capacitor. For this development, the only known parameters are charge, $Q(t)$, current, $I(t)$, and desired power output, $P(t)$. Here we express Q, I, and P as $Q(t)$, $I(t)$, and $P(t)$, respectively, to emphasize that they are functions of time.

We present the following fundamental principles of Ohm's Law because it is the foundation for the developments of metrics and parameters for reverse engineering, as pre-

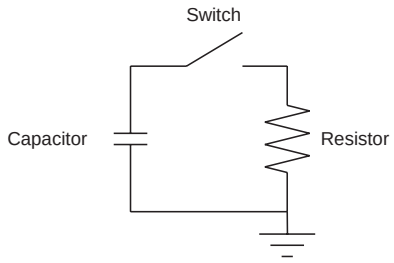

Figure 3.1: Simple resistor-capacitor circuit. The capacitor is initially fully charged and begins to discharge the instant the switch is closed at $t = 0$.

sented in Chapter 4. Ohm's law characterizes the relationship between resistance, current, and voltage in a circuit and can be expressed as

$$R = \frac{V(t)}{I(t)} \tag{3.1}$$

while the capacitance, C, of an element can be expressed as [48]

$$C = \frac{Q(t)}{V(t)} \tag{3.2}$$

where $V(t)$ represents the voltage difference across the resistor at current $I(t)$, and $Q(t)$ represents the charge stored in the capacitor. Notice that while V, I, and Q are time dependent, R and C are not. This important principle is used later in the thesis to assist the designer in specifying reverse engineering parameters.

The resistance and capacitance of the circuit can be conveniently expressed in terms of Q, I, and P when the following well-accepted [49] relation is considered. Specifically when

$$P(t) = I(t)V(t) \tag{3.3}$$

it follows that

$$R = \frac{P(t)}{I(t)^2} \tag{3.4}$$

and

$$C = \frac{Q(t)I(t)}{P(t)}. \tag{3.5}$$

As shown in subsequent sections of this thesis, this form of the resistance and capacitance relationships is particularly useful in the context of information extraction during reverse engineering.

When R and C are known for a given system, the time to discharge a capacitor can be quantified as a function of the charge remaining in the capacitor by

$$T = -RC \ln\left(\frac{Q}{Q_0}\right) \tag{3.6}$$

where it is assumed that the capacitor begins to discharge at $t = 0$, and T represents the time when the specified charge, Q, is remaining in the capacitor where Q_0 is the quantity of charge initially stored by the capacitor. As Eq. 3.6 is an exponential relationship, the time to fully discharge the capacitor is infinite. For this reason, Q is often selected to be a positive non-zero value with the bounds

$$0 < Q \leq Q_0 \tag{3.7}$$

which results in a finite quantity of time.

Therefore, by these relationships, any resistor-capacitor circuit can be analyzed and, importantly, a prediction of time to discharge the circuit's capacitor can be made. Additionally, by using Ohm's law as a basic building block, circuits of any complexity can be analyzed using well structured, well-known, approaches such as Kirchhoff's current and voltage laws [49]. As presented in Chapter 4, we use this same basic relationship to estimate the time required to discharge information about a product, from the product itself.

Chapter 4

Development of Metrics and Parameters for Reverse Engineering

In this chapter, we present metrics and parameters for characterizing the barrier and time to reverse engineer any product. The presentation of the metrics and parameters is divided into three main parts in this chapter. Section 4.1 presents the general relationship for barrier and time to reverse engineer any product, with a brief description of the supporting parameters and metrics. Section 4.2 provides practical insight into specifying the needed parameters, and quantifying barriers and time for small subsets of a larger problem. Section 4.3 shows how the solutions to these small subsets can be reintegrated to solve the large problem.

4.1 General Metrics for Reverse Engineering

The barrier, B, to reverse engineer a product can be expressed as

$$B = \frac{P}{F^2} \tag{4.1}$$

where P is the power – effort per time exerted to extract information – and F is the rate at which information can be extracted from a product. The time, T, to reverse engineer a product is

$$T = -BS\ln\left(\frac{K}{K_0}\right) \tag{4.2}$$

where K is the information contained by a product at a specific moment in time and K_0 is the information initially contained by a product. For simplicity, K is often defined as a fraction of K_0 (i.e., $K = 0.05K_0$ for the examples presented in this thesis). Specifically, the

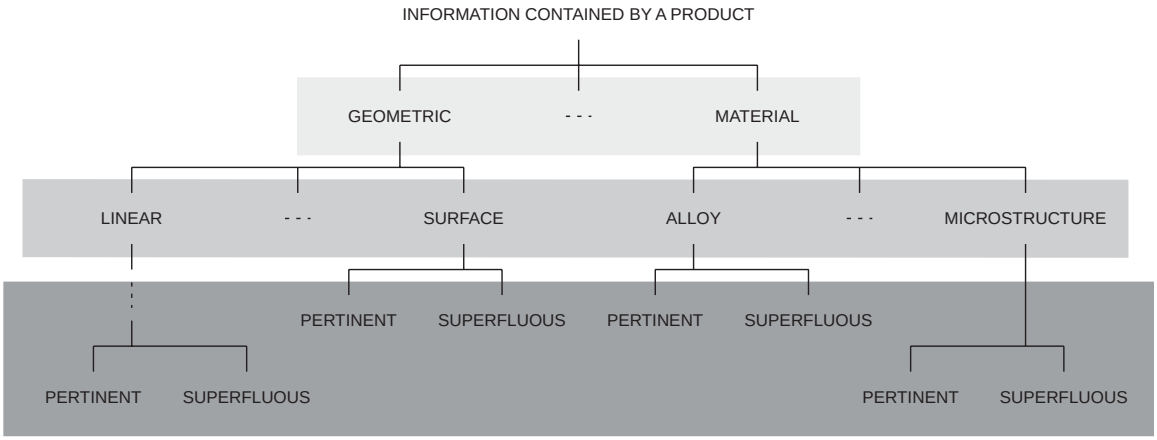

Figure 4.1: A basic taxonomy of information contained by a product.

quantity K is constrained to

$$0 < K \leq K_0 \tag{4.3}$$

which ensures that Eq. 4.5 yields a finite quantity of time. The quantity S in Eq. 4.5 is evaluated as

$$S = \frac{KF}{P} \tag{4.4}$$

where S is termed *information storage ability* of a product, which is analogous to electrical capacitance. When K, K_0, F, and P are the known input parameters, T can be expressed as

$$T = -\frac{K}{F} \ln\left(\frac{K}{K_0}\right) \tag{4.5}$$

indicating that one can increase the time to reverse engineer a product by either increasing the quantity of information contained by a product or decrease the rate at which that information can be extracted.

4.2 Decomposition of a Product for Barrier and Time Analysis

In a realistic setting, it can be difficult to accurately determine the values of K, F, and P for the product as a whole. However, a product can be decomposed into disparate information components allowing for a more simple quantification of K, F, and P for each component. In this section, we present an approach for decomposing a product based on

information components, and analyzing each component to determine B and T. In Section 4.3, we discuss how the quantities B and T for each component can be systematically combined to determine the total barrier, B^*, and the total time, T^*, to reverse the product as a whole.

We start by discussing the parameter K, and the categorization of it. Recall that K is the estimated or actual information contained by a product, and that the purpose of reverse engineering is to extract information contained by a product from the product itself. Some examples of information contained by a product include material, geometry, electrical conductivity, and color. While there are many different ways a product can be decomposed, we present a process by which products are decomposed according to categories of information contained by the product. For the purposes of this thesis, information contained by a product, K, is categorized according to the taxonomy chart in Figure 4.1.

As seen in the taxonomy chart, the general information contained by a product can be separated into three basic levels. At the highest level, information is categorized into information types such as geometric information and material information. The second level of categorization separates each information type into information classes. For geometry, information classes include linear dimensions and radial dimensions, among others. When applicable, another categorization of geometric information class can include micro dimensions, meso dimensions, and macro dimensions. The final level of categorization on the taxonomy chart is the information sub-class which only has two categories – information that is pertinent to product performance and information that is superfluous. Generally speaking, the product should be decomposed into the minimum number of levels needed to easily specify the parameters K, F, and P for all the information contained by the product. As values for K, F, P, S, B, and T are specified or calculated for each information type, a subscript $[\,]_i$ is used to distinguish information types or information classes – depending on the level for which K, F, and P are being analyzed – while the superscript $[\,]^*$ represents the values of $[\,]$ that pertain to the product as a whole.

With the different information types defined, K is more fully defined as the *estimated*, *unextracted*, *pertinent* information contained by a product *at a specific time*. The quantity of information contained by a product is therefore a function of information type,

i, and time, t. The quantity of pertinent information contained by a product is determined as the number of relevant units of information that is critical to the performance of the product.

For convenience in specifying the parameters K, F, and P, we define two reference time frames. Time in the t domain is the traditional representation of time, which captures any moment during the reverse engineering process. As it may be difficult to determine the quantity of pertinent information contained by a product, and the rate at which it is extracted, at any time t when the product contains both pertinent and superfluous information, a second reference time frame is used. This second reference time frame, in the domain τ, is a theoretical time frame when all the values of K, F, and P are known, and all information is deemed pertinent. In the τ time frame, the time-independent quantities of B and S are more easily calculated. Since these quantities are time independent, they can also be used directly in the t time frame where there exists many unknown factors.

We pause now to make a clear distinction between $K(\tau)$ and $K(t)$. The parameter $K(t)$ represents only the pertinent information contained by a product, while the parameter $K(\tau)$ represents the *total* information contained by a product, be it pertinent or superfluous. In general, the most conservative value of $K(\tau)$ is when $K(\tau)$ is set equal to $K(t)$ implying that competitors know exactly what information is pertinent and what is superfluous. The quantity $K(\tau)$ is principally used for calculating S. A similar process of using two different reference frames is often used to determine the capacitance and resistance of electrical elements. If a resistor value is unknown, one can apply a known voltage and measure the current and determine the resistance of the system using Ohm's law. The resistance of a resistor is not dependent upon electrical current, voltage, or time. Therefore the resistance may be known for all times, t, once it is known for a single time, τ, where a known voltage and current has been applied.

When a product is reverse engineered, no amount of superfluous information will benefit those extracting the information. For this reason we are only interested in the rate, F, at which *pertinent* information can be extracted. For a product that contains both pertinent and superfluous information, it may be difficult to determine the flow rate of pertinent information when both pertinent and superfluous information is being extracted. For this

reason, the flow rate of information is determined in the τ reference frame where all information is assumed pertinent. The quantity $F(\tau)$ is principally used for calculating S and B for individual information types.

Typically when extracting information contained by a product, the information that is quickly and easily extracted is extracted at a high flow rate. At times in the information extraction process, information becomes more difficult to extract resulting in a lower flow rate. It is also apparent that the flow rate of one information type such as geometric linear dimensions may not be the same flow rate as another information type such as material grain orientations. The flow rate of information in the τ reference frame can be determined experimentally by measuring the time to extract information of particular knowledge classes, such as geometric linear dimensions.

The measure of effort per time exerted to extract information contained by a product is characterized as power, P. The quantity P is also determined in the τ reference frame and is used in calculating both S and B. The value of P is constrained by

$$0 < P \leq 1 \tag{4.6}$$

where zero represents no effort being put forth to reverse engineer a product and one signifies maximum effort is exerted. The value of power should be selected to accurately represent the effort per time the competitor will exert while reverse engineering the product and, for this study, is assumed to remain constant – at a value of one – during the analysis of a given product and competitor. With the values of K, F, and P defined, B and S can be calculated according to Eqs. 4.1 and 4.4 for each information type i or for the product as a whole if it can be evaluated as a whole. When the product cannot be evaluated as a whole, the developments of the next section become important.

4.3 Integration of Analyses for Overall Product Evaluation

In this section, the total time to reverse engineer, and the total barrier to reverse engineering, are calculated by strategically combining the barrier and time to reverse engineer each information component as discussed previously. In the previous section, we discussed

how a product can be decomposed to facilitate the selection of K, F, and P resulting in a B and T for each information type. To estimate the barrier and time to reverse engineer the product as a whole, we perform an analysis on a pseudo product that has the same performance as one that has the considered information types combined enabling an estimation of B and T for the entire product.

The total time, T^*, to reverse engineer a product, the total information, K^*, contained by a product, and the total storage ability, S^*, of a product can be determined by

$$T^* = \sum_{i=1}^{N} T_i \tag{4.7}$$

$$K^* = \sum_{i=1}^{N} K_i \tag{4.8}$$

and

$$S^* = \sum_{i=1}^{N} S_i \tag{4.9}$$

where N is the quantity of information types the product has been decomposed into.

When individual information types are analyzed, the known values include F and P. With the pseudo product, however, the flow rate is calculated by

$$F^* = \frac{K^*}{T^*} \tag{4.10}$$

which enables P^* to be calculated as

$$P^* = \frac{K^* F^*}{S^*} \tag{4.11}$$

when the values of K^*, F^*, S^*, and T^* are used for both Eqs. 4.10 and 4.11. Note that Eq. 4.11 is obtained by rearranging Eq. 4.4 and solving for P.

Only now that the effective rate at which information can be extracted from the pseudo product and the power required to extract information are known, the effective barrier for the entire product can be determined by using Eq. 4.1. It is important to note that the barrier and time to reverse engineer a product is dependent upon skills and resources

available (both affecting the flow rate of information). Therefore the barrier to reverse engineer a product may vary depending upon the group performing the reverse engineering activities [52].

The accuracy of the time and barrier to reverse engineer a product is dependent upon accurate selection of the parameters K, F, and P. Depending upon the reverse engineering perspective taken, some parameters may be more accurate lending to a better estimation of the time and barrier to reverse engineer a product. Recall that there are at least two practical reverse engineering perspectives: that of the original designer who seeks to determine, and even maximize, the difficultly to reverse engineer their product; and that of the competitor who seeks to reverse engineer the innovative product.

When the original designer uses the relationships presented in this thesis, he/she is able to accurately determine the actual quantity of pertinent information, K, contained by the product but will only be able to estimate the rate at which the competitor can extract information, F. The competitors, on the other hand, will be able to accurately determine the rate at which they (the competitors) can extract information, F, but will be forced to estimate the initial quantity of pertinent information contained by the product. Additionally, it may not be obvious to the competitor which information is pertinent and which is superfluous – especially if the designers developed the product to be difficult to reverse engineer. It is likely that the original designers can estimate information extraction rate for the competitors more accurately than the competitors can estimate the quantity of pertinent information contained by a product. A simple approach would be for the original designer to specify a flow rate of information extraction based on their own skill and motivation, as it is likely that their competitors have similar skills and motivation.

Chapter 5

Empirical Validation of Developed Metrics

In this chapter, we present an empirical study with the purpose of showing that the time and barrier to reverse engineering can be estimated by the relationships presented in this thesis for products of sufficient complexity. For this study, only geometric information is extracted and analyzed.

There are four major parts to reverse engineering and all have affect the flow rate of information extraction: planning, measuring, recording, and verifying. During the reverse engineering process, time is not only spent extracting pertinent information, but time is also spent recording the data, developing a plan of information extraction, and verifying that all of the information has been extracted and that the information has been accurately extracted.

For any information type, the time to extract a unit of information varies from unit of information to unit of information (within a product) and from product to product. In part, this is due to time not only spent on extracting pertinent information, but time is also spent recording the data, developing a plan of information extraction, and verifying that all of the information has been accurately and complectly extracted. An effective and efficient way to handle the differing times is to determine an individual's general rate of information extraction [53]; by general we mean valid for all product complexities. Note that the general information extraction rate is strictly a measure of the rate at which the individual extracts information without consideration to time spent planning, recording, or verifying. However, when the general information extraction rate used in the exponential time estimation presented in Equation 4.5 it has been found to estimate the total time to reverse engineer a product (including time spent planning, recording, and verifying) with

Figure 5.1: Part 127 as presented in Chapter 5.

an average error of 12.2%. As a note, the general extraction rate is the rate of information extraction $F(\tau)$ as described in Section 4.2. We obtain $F(\tau)$ for geometric information experimentally by issuing a uniform dimension extraction test in the form of a computer program that we created. The test is set up to allow the individual to familiarize themselves with the dimension to be extracted then they are instructed to extract that dimension with a measurement tool while the time is recorded. The recorded time, therefore, only is only a measures of information extraction as the planning, recording, and verifying is performed for the user by the computer program. This process is repeated multiple times for different dimensions to determine the general rate at which the individual extracts dimensions.

To illustrate, four individuals were asked to reverse engineer Part 127 and Part 128 as seen in Figure 5.1 and Figure 5.2, respectively. Before beginning the reverse engineering process, the information extraction rate was determined for each individual. The individuals were then instructed to extract and record the dimensions with enough detail that the product could be recreated if needed.

The plots seen in Figure 5.3 and Figure 5.4 are the results of a single individual for both products and compared to the linear and exponential time approximations with the linear relationship is defined as

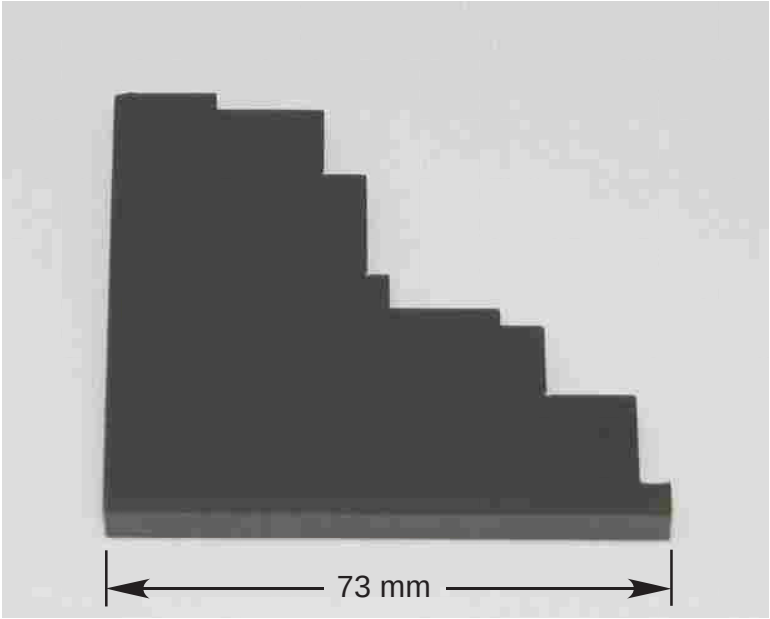

Figure 5.2: Part 128 as presented in Chapter 5.

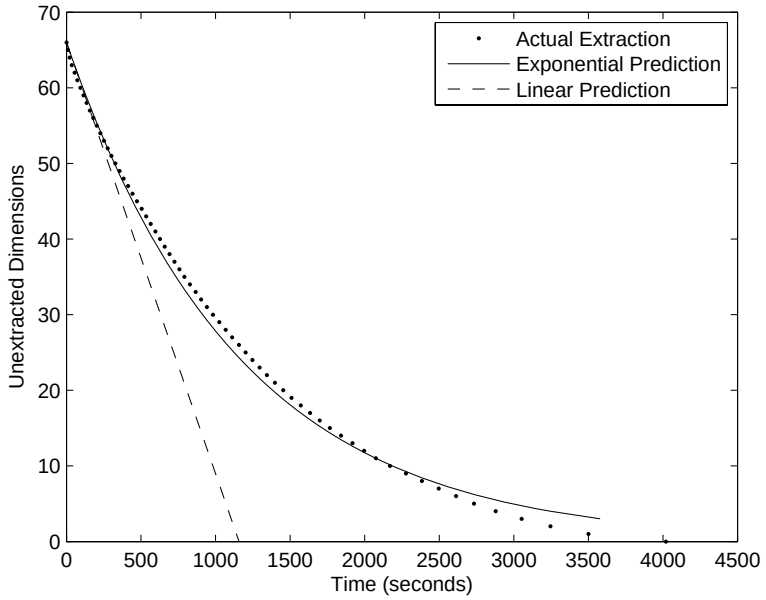

Figure 5.3: Plot of unextracted dimensions remaining in Part 127 vs. time as compared to the linear and exponential time predictions for Individual 1.

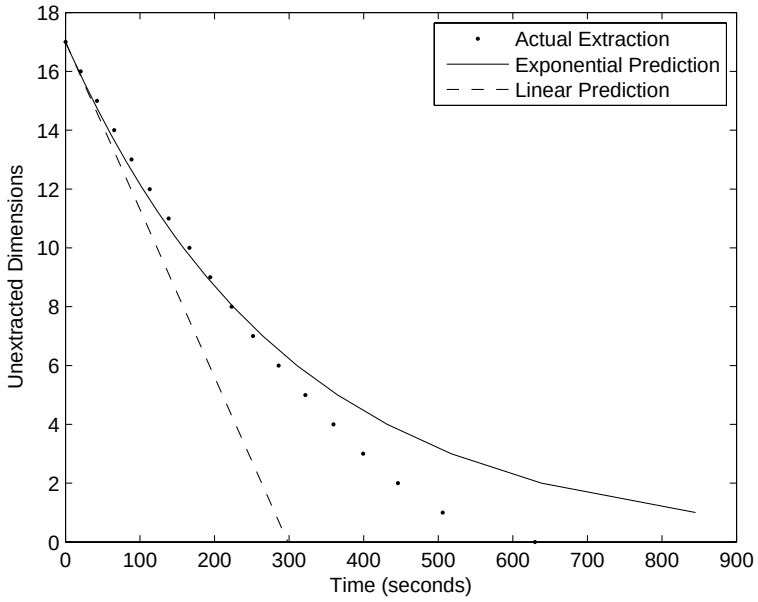

Figure 5.4: Plot of unextracted dimensions remaining in Part 128 vs. time as compared to the linear and exponential time predictions for Individual 1.

$$T = \frac{K}{F} \tag{5.1}$$

where the information extraction rate (F) of the individual is the slope and the number of dimensions (K) to be extracted is the y-intercept on a plot of dimensions versus time. While the plots are for a single individual, they are representative of all the individuals that reverse engineered the products and are consistent with other tests we have performed. The data in the plots has been rearranged according to the time to extract each dimension - with the shortest times plotted first - and are not plotted in the order of dimension extraction. Tables 5.1 and 5.2 present the predicted time to reverse engineer each product, for each individual, as well as the calculated barrier to reverse engineering. From Tables 5.1 and 5.2 we see that the barrier to reverse engineering is the same for both parts for each individual. This is due to the fact that the barrier is only dependent upon the individual and the type of information being extracted and not dependent upon the quantity of information extracted.

To determine the validity of the relationships presented, multiple individuals have reverse engineered multiple products resulting in over fifty sets of data for geometric in-

Table 5.1: Table of predicted and actual times to extract geometric information from Part 127. Time is in seconds.

Individual	Actual Time	Linear Prediction	Linear % Error	Exponential Prediction	Exponential % Error	Barrier
1	4020	1158	-71.20%	3579	-10.97%	307.8
2	3473	847	-75.60%	2656	-23.51%	339.2
3	1367	517	-62.19%	1433	4.84%	260.9
4	2201	826	-62.48%	2323	5.55%	272.8

Table 5.2: Table of predicted and actual times to extract geometric information from Part 128. Time is in seconds.

Individual	Actual Time	Linear Prediction	Linear % Error	Exponential Prediction	Exponential % Error	Barrier
1	629	298	-52.65%	845	34.16%	307.8
2	568	298	-44.48%	887	56.20%	339.2
3	595	242	-59.28%	656	10.27%	260.9
4	522	264	-49.33%	733	40.49%	272.8

formation extraction. By observation and data analysis, we have verified that the time to reverse engineer the geometry of a product can be approximated by an exponential relationship. We have also observed that simple products tend to be less accurately estimated by the exponential relationship. Part 128 was specifically selected to test the exponential relationship near the limits of application and it may be seen that a linear approximation may be more accurate for the simplest of parts. However, Part 127, while still relatively simple, has been found to be sufficiently complex to be accurately estimated by the exponential relationship.

Products of higher degrees of complexity have also been analyzed and have also been found to be accurately represented by the exponential relationship. To illustrate this, we briefly discuss the reverse engineering of Apple Inc.'s recently released computer keyboard as seen in Figs. 5.5 and 5.6. As with the previous examples, we will only reverse engineer geometry and do not reverse engineer the material properties or the keyboard electronics. However, if the flow rate of information extraction is determined for extracting material properties and analysis of electronics, the same relationships used for estimating

Figure 5.5: Figure of keyboard before disassembly.

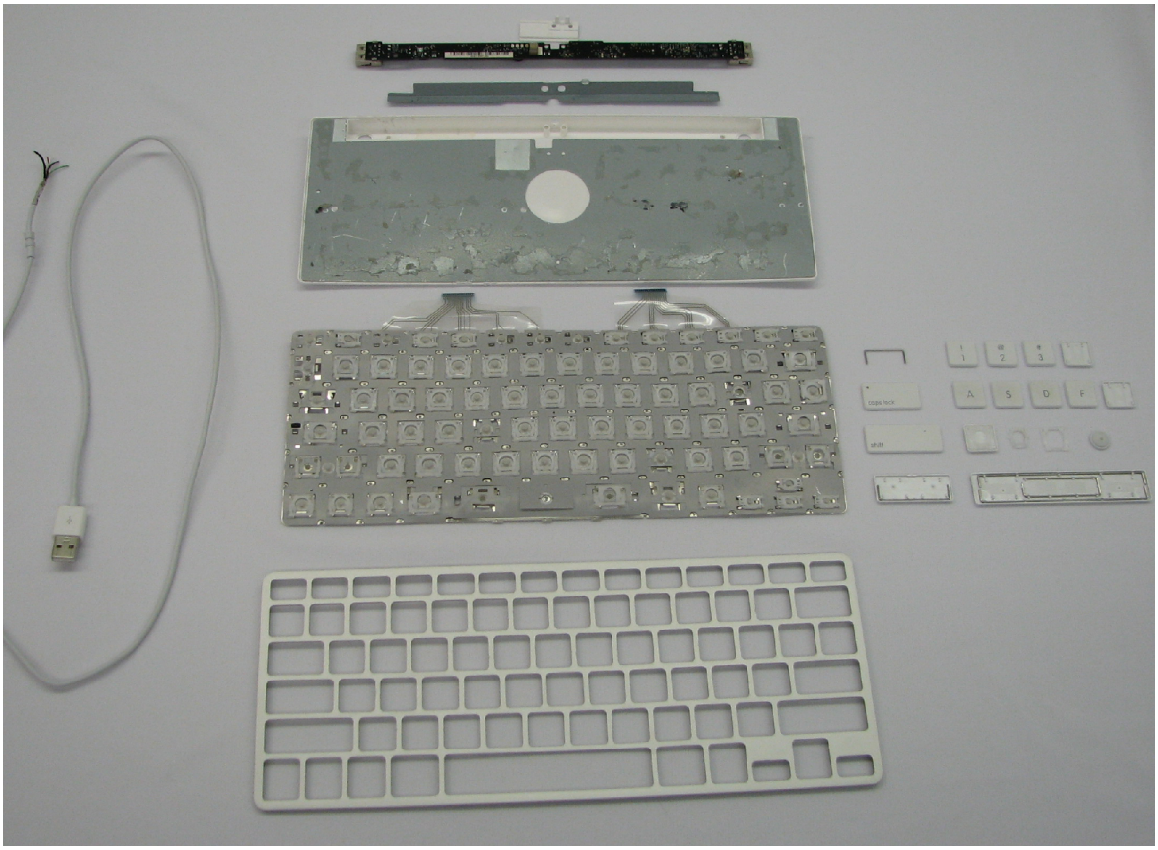

Figure 5.6: Figure of keyboard disassembled.

the time and barrier to extract geometric information can also be used to estimate the time and barrier to extract information about material properties and the electronics of a system.

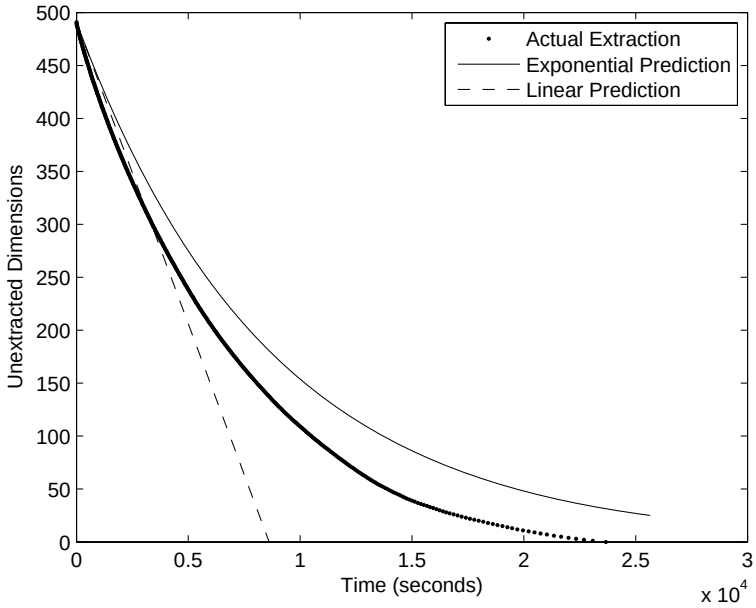

Figure 5.7: Plot of unextracted dimensions remaining in keyboard vs. time as compared to the linear and exponential time predictions.

We reverse engineered the keyboard to the degree that we could recreate keyboard parts that would be interchangeable with the current product. In order to fully extract the geometric information contained by the keyboard, some disassembly was required. While disassembly time may be important to quantify, it was not the focus of this study or of the developed metrics. Therefore, the keyboard was considered disassembled when reverse engineering began. Utilizing the relationships presented in this thesis to estimate the time and barrier to reverse engineer the keyboard resulted in a barrier of 307.8 and an estimated time of $25,649$ seconds. In actuality, it took $23,667$ seconds to reverse engineer the keyboard - an 8.38% error when compared to the predicted time. The estimated and measured times were determined independently so that neither influenced the other. Figure 5.7 compares the actual time to reverse engineer the keyboard with the exponential and linear predictions.

In this chapter we have shown how the reverse engineering time and barrier is calculated for various products. While it is useful to characterize a product's time and barrier, designers typically desire to impede or entirely prevent reverse engineering attempts. In the next chapter we discuss a design strategy that results in effective barriers to reverse en-

gineering built into product components. Specifically, we discuss how material microstructures can be critically oriented and coupled with geometry to obtain an unexpected and desired performance effectively increasing the barrier to reverse engineering.

Chapter 6

Enabling Technologies for Constructing Barriers to Reverse Engineering through Microstructure Manipulation

Recall that the purpose of this thesis is to develop a design methodology that increases the time and barrier to reverse engineer hardware. One effective way to increase the barrier is to develop products that perform in an unexpected, but desirable manner. In this chapter, we present the technology and theories that enable products to exhibit this unexpected performance resulting in a large barrier to reverse engineering.

For many product designers, material properties, such as yield strength, σ_y, and Young's modulus, E, are chosen from a set of discrete values, typically published in the form of a material properties table [54]. Under this typical approach, if one requires a part to withstand more stress before failure, the geometry is typically changed or a new material class or alloy is selected. Consider the benefit that would come to the design engineer if he or she could hold the geometry constant and, using the original material, improve the material's yield strength or other material properties. He or she could increase product performance without resorting to more expensive materials or they could hide performance increases from competitors, since discovering the source of the increased performance would not be trivial. The following sections present a methodology to do this.

Recent advancements in material science enable the development of the proposed approach. Specifically, it is the advancements pertaining to material microstructure, which is the composition of a material including arrangement, size, orientation and distribution density of crystallographic grains [55], that enable material properties to be treated as continuous design variables. These advancements have led to predictive relationships for characterizing material properties as a function of the material microstructure. When coupled

with numerical optimization and lamination technology (two other key enablers), material properties can be modified as simply as geometry, creating one more degree of freedom in the design. Additionally, the method outlined in this thesis allows one to make calculated changes to the microstructure to obtain desired results in material properties at designer specified locations (heterogeneously) or across the entire part (homogeneously).

It is known that one or more microstructures can be used as a starting point to obtain combination of properties in the property closure, which is the set of all theoretically possible material properties [55]. Unfortunately, it is not known how to consistently manufacture all microstructures required to obtain every combination of properties in the property closure. Therefore only a small, discrete, set of material properties contained within the full property closure are commonly used in practice. This is one of the main reasons why material properties are rarely considered continuous variables in the material selection activities of product design. With the use of laminations, microstructures that were previously difficult to obtain become simple combinations of optimally-layered, well-known microstructures [39] as presented in this thesis. This process is similar to carbon-fiber composite materials where many thin layers are ideally aligned to obtain desired material properties in specific directions [56].

In this chapter we present the enabling technology of ultrasonic consolidation [40] which facilitates the joining of thin metal sheets with minimal disturbances to the microstructure in the weld areas. We also present four fundamental theories required for predicting material properties for a part, based on measurements of a material's microstructure. They are: reference frames, fundamental zone, rotations of anisotropic layers, and the lamination of those thin layers.

6.1 Ultrasonic Consolidation: Additive Manufacturing Process of Metals

One manufacturing technology that allows improved material properties to be obtained from common metals is the additive manufacturing process of ultrasonic consolidation (UC). UC utilizes principles of ultrasonic welding [40] to combine metal sheets, typically 150 μm thick, in a layer-by-layer process. This process is often combined with a 3-axis CNC mill to produce complicated geometry during the additive process. The UC

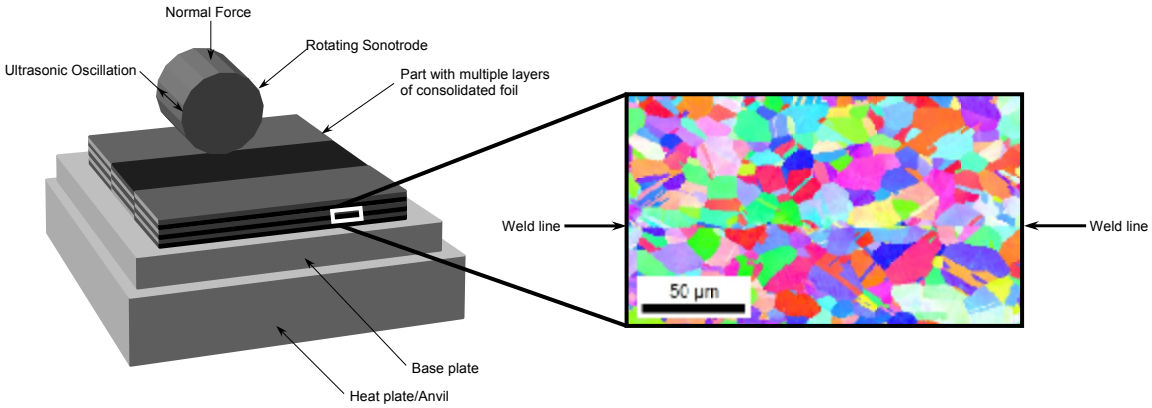

Figure 6.1: Ultrasonic consolidation process with scanning electron microscope image of grains at layer interface.

process, as represented in Figure 6.1, begins with a heated base of the same material of the part. A rolling/rotating sonotrode applies a normal force while oscillating which results in dynamic interfacial stresses at the interface between the two mating surfaces [40, 57, 58]. The stress incurred by the high frequency oscillations, around 20 kHz, produce elastic-plastic deformation and establishes a metallurgical bond as can be seen in the polished crossection shown on the right-side of Figure 6.1. This process is repeated layer-by-layer until the part is completed with the desired number of layers. It is impressive to note that UC materials can yield a 85% to 100% linear weld density along the bonded interface [59].

One important characteristic of UC is the low temperature at which the layers are welded together, which range from ambient to $350^{\circ}F$. This results in minimal local disturbances in the weld area, thus making the layer-by-layer construction virtually undetectable, which supports the notion of hiding the source of performance increases from competitors.

Possibly the most impressive feature of UC is the number of microstructures that may be obtained thereby. It is known that extreme microstructures may be induced in metal foils by rolling and recrystallization [60]. These foils may then be combined by the UC process to create a material made with laminations. When layers with known microstructures are strategically placed, one can effectively create a laminated material with desired properties and even consistently obtain material properties that are otherwise not used in practice.

6.2 Reference Frames and Fundamental Zone Defined

In this section we define three reference frames commonly used when working with laminae: Crystal, Laminate, and Part reference frames. The main purpose of these reference frames is to have a consistent point of reference when aligning layers and defining directionally-dependent material properties. While it is important that reference frames do not vary within a sample or part, it does not matter how reference frames are oriented. Often it is useful to align reference axes with either the sample's geometry or the sample's texture. Typically the crystal's reference frame will be aligned with the crystallographic directions, X_{cj}, Y_{cj} and Z_{cj} for the j-th crystal in a sample, [61] where the subscript c represents the crystal frame.

A convenient reference direction for a heavily rolled lamina is the rolling direction. One axis of the sample reference frame is aligned with the rolling direction and is termed "*Rolling Direction*" or D_k^R for the k-th layer. The second axis, or "*Normal Direction*" (D_k^N), is placed perpendicular to the both the rolling direction and a surface of the laminate. While it does not matter which surface is selected for the thin lamina, typically surfaces with a large surface area are used as the reference. With two axes defined, the third axis, the "*Transverse Direction*" (D_k^T), is defined with the use of the right-hand rule [55].

The final reference frame to be described, the part reference frame, is defined according to the geometry of the part as seen in Figure 6.2 as X_p, Y_p and Z_p. The part reference frame allows one to properly align the laminae rotations to achieve the desired properties in the directions of interest [61].

The orientation of one reference frame to another is represented by the standard Euler angles, ϕ_1, Φ, and ϕ_2. The Euler angles represent all possible orientations but due to symmetry, the limits on the angles may be set to $0 \leq \phi_1 < 2\pi$, $0 \leq \Phi \leq \pi$, and $0 \leq \phi_2 < 2\pi$ respectively [61]. For parts constructed with layers, it is convenient to only rotate the layers about their normal axes which is what we do in this thesis.

Another important concept in being able to extract material properties from crystal orientation data is the Fundamental Zone (FZ). The FZ is the set of all physically-distinct orientations of the local crystal that can occur [55]. Due to the computational power required to analyze the infinite number of possible crystal orientations, the FZ is binned into

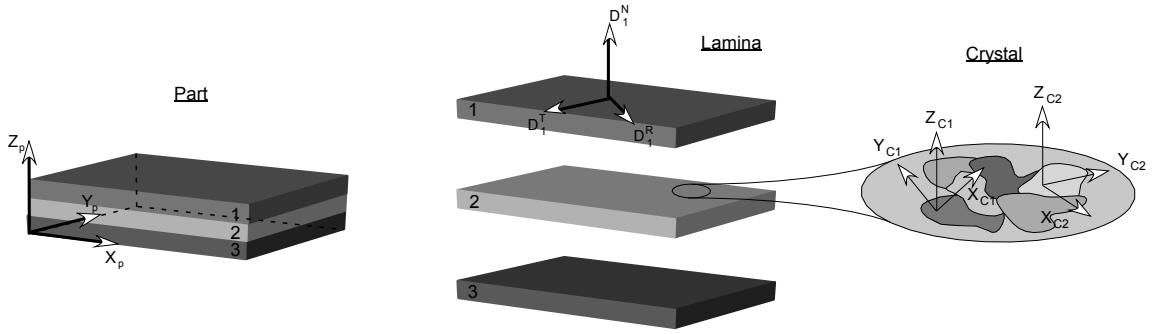

Figure 6.2: Reference frames defined for the part, lamina, and crystal.

groups of orientations with each bin approximated by a single orientation. The Binned Fundamental Zone (BFZ) can then be used as a simplified orientation description for all crystals in the sample. The number of bins is determined by the conflicting objectives of desired accuracy and computational time available.

6.3 Using the Rotation and Lamination Theory to Predict Material Properties

In this section we present the process by which material properties may be determined given knowledge of the material microstructure.

The microstructure-to-material-property theory is the process by which the material properties are predicted, given information about the microstructure. In the rotation and lamination theory presented below, it is through manipulation of the material microstructure of each layer that one is able to obtain an overall change in material properties and product performance. Therefore, it is important to understand the microstructure-to-material-properties theory which is the crucial link in considering material properties as continuous variables. The reader is referred to [62] and [39] for the full development of the microstructure-to-material-property theory and the rotation and lamination theory as presented in this section.

The flowchart in Figure 6.3 presents the process in which material properties are determined from microstructure properties of a material. The process contained by the dashed box determines yield strength and the process contained by the solid box determines

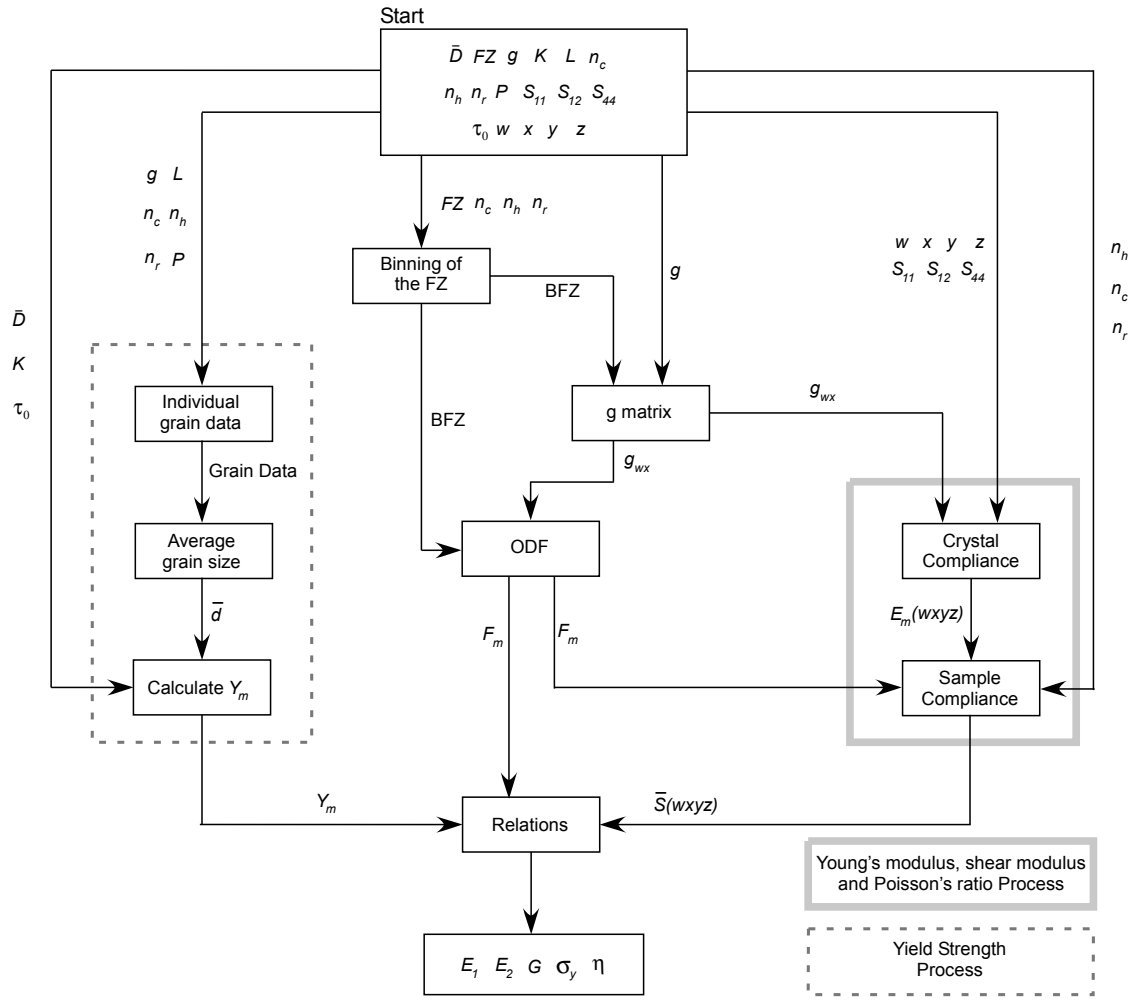

Figure 6.3: Microstructure-to-material-properties flowchart. Note that K in this figure represents the Hall-Petch slope, and P represents crystal slip planes.

Young's modulus, shear modulus, and Poisson's ratio. The remaining steps are required for both processes. The flowchart in Figure 6.3 is now described in detail.

6.3.1 Procedure Required to Determine all Material Properties

The process begins by initializing the variables shown in the uppermost box of Figure 6.3 and obtaining the material specific constants from literature such as S_{11}, S_{12}, and S_{44} [63]. Next the FZ is binned allowing multiple orientations to be approximated by a single orientation thus decreasing the number of orientations needing analysis. The resolution

of the binning is determined by dividing the FZ into a number of rows, columns, and layers represented by n_r, n_c, and n_h, respectively. Fewer bins equates to a faster computational time with a decrease in accuracy while increasing the number of bins improves accuracy at the expense of time. The Fourier coefficient F_m can then be calculated which is literally the volume fraction of crystals in the m-th bin of the BFZ. Simply stated, F_m is the percentage of crystals that are aligned in a given direction and is used for calculating yield strength, Young's modulus, shear modulus, and Poisson's ratio. Before F_m can be calculated, crystal orientation data (g) obtained by Orientation Image Microscopy [55] (OIM) is imported into the BFZ to be converted into matrix form (g_{wx}) as represented by the box titled "g matrix" in Figure 6.3. One of the key factors in obtaining a continuous range of material properties is the understanding of the initial microstructure as determined by OIM. Without the details of the starting microstructure for the specific material to be used, the desired material properties cannot be obtained with the rotation/lamination theory.

6.3.2 Procedure Specific to Determining Yield Strength

Now we consider the important step of predicting material yield strength as a function of the material microstructure as seen in Equation 6.1 and Equation 6.3. For the sake of this thesis, sequential equations have been condensed to a single equation as seen in Equation 6.1

$$\overline{D}_{ij} = D_{ij} = \dot{\gamma}_0 \sum_{s=1}^{S} \left| \frac{(\sigma'_{kl})\mu_{kl}^{(s)}}{\tau^{*(s)}} \right|^n sign\left((\sigma'_{kl})\mu_{kl}^{(s)}\right)\mu_{ij}^{(s)} \tag{6.1}$$

where $\overline{D}_{ij}$ is an imposed macroscopic (pertaining to the layer or part as a whole) strain rate, [64] D_{ij} is a tensor representing the local (pertaining to the crystal only) strain rate and assumed to be equivalent to the macroscopic strain rate according to the Taylor hypothesis [65], $\dot{\gamma}_0$ is the reference shear rate, S is the total number of slip systems in the material, σ'_{kl} is the local deviatoric stress for a given direction, [66] $\mu_{kl}^{(s)}$ and $\mu_{ij}^{(s)}$ are simple combinations of the slip directions and the slip plane normals, [66] and $\tau^{*(s)}$ is the reference shear stress as calculated from the Hall/Petch relationship [67].

All of the values in Equation 6.1 are known with the exception of the local deviatoric stress, σ'_{kl} which requires a Newton-Raphson method, or a similar non-linear solving method, to numerically determine the local deviatoric stress. According to the Taylor model used, the macroscopic deviatoric stress may then be related to the local deviatoric stress according to Equation 6.2

$$\left\langle \sigma'_{kl} \right\rangle \approx \overline{\sigma}'_{kl} \tag{6.2}$$

where $\left\langle \sigma'_{kl} \right\rangle$ represents the volume average of the local deviatoric stress and $\overline{\sigma}'_{kl}$ represents the macroscopic deviatoric stress. With the macroscopic deviatoric stress calculated, the yield strength may be predicted according to Equation 6.3.

$$\sigma_{y1} = \bar{\sigma}'_{11} - \bar{\sigma}'_{22} \tag{6.3}$$

For the full development and application of Equation 6.1 and Equation 6.3 the reader is referred to Adams et. al., [62] Fromm et. al., [66] Taylor, [65] and Asaro and Needleman [68].

We now consider the dashed box on the left-hand side of the flowchart in Figure 6.3. Given Euler angles, g, the binning information for the FZ (n_r, n_c, n_h), crystal structure slip planes (P) such as (111) for Face-Centered-Cubic materials, and L (resolution at which average grain size is determined), [66] the average grain size, $\overline{d}$, may be obtained as seen in the box labeled "Average grain size." To be consistent with the material science literature, the crystal structure slip planes is termed P and the Hall-Petch slope is termed K in the relevant figures in this chapter and should not be confused with P and K as defined in the nomenclature. With the average grain size known, Y_m may be calculated with the input of $\overline{d}$, lattice friction stress, τ_0, Hall-Petch slope, and the average strain tensor $\overline{D}$ according to the flowchart in Figure 6.3. Once Y_m is known, the yield strength, σ_{y1}, of the material can be calculated according to the equations described above.

6.3.3 Procedure Specific to Determining Young's Modulus, Shear Modulus and Poisson's Ratio

The remaining three outputs all depend directly on the compliance of the sample in the direction of interest. Like the process for determining yield strength, one starts by binning the FZ and creating an orientation matrix for each bin. Next, a Fourier coefficient representing a simple decomposition of the crystal compliance (S) in the desired direction can be computed which is named E_m with m representing the m-th bin in the BFZ.

The simplest way to determine the percentage of crystals in a bin is with the use of the Orientation Distribution Function (ODF). The ODF is a function that receives information about the BFZ and Euler angles, g, enabling a description of all crystal orientations in a sample. Calculating the ODF with a single direction results in a scalar representing the percentage of crystals aligned in that direction. When the ODF is calculated for multiple directions, the results are a scalar representing the percentage of crystals aligned in the multiple directions defined – such is the case of a bin in the BFZ.

As is true with all material properties, compliance of the sample is driven by the compliance of each crystal. In fact, the sample compliance, $\overline{S}_{wxyz}$, is simply an average compliance of all crystals. Inputs required to determine crystal compliance are the direction of interest as defined by the designers (w, x, y, z) and three material properties which comes from literature; S_{11}, S_{12}, and S_{44}. With F_m and E_m known, it is a simple matter to input the total number of bins and compute $\overline{S}_{wxyz}$. Similar to Y_m being related to σ_y, $\overline{S}_{wxyz}$ can be related to Young's modulus, shear modulus and Poisson's ratio by Equation 6.4 and Equation 6.5 [69].

$$S_{1111} = \frac{1}{E_{1111}} \tag{6.4}$$

$$E = 2G(1+\nu) \tag{6.5}$$

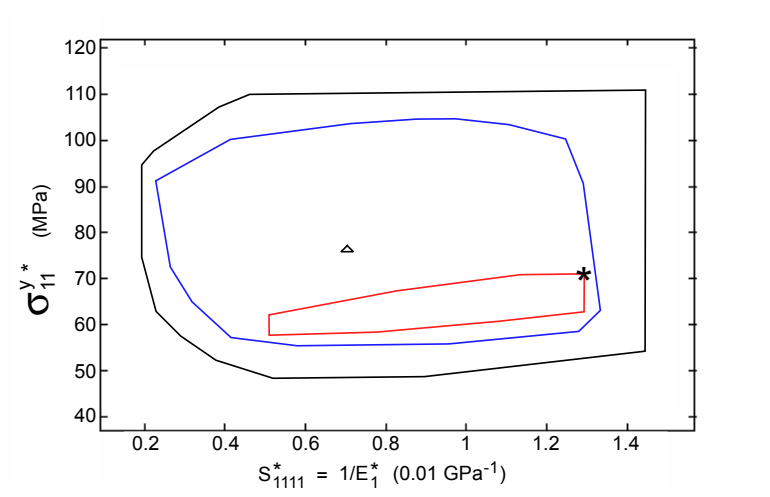

Figure 6.4: Property closure of yield strength vs. compliance for Ni 201 for various microstructures.

6.4 Part Construction by the Rotation and Lamination Theory

We now consider approaches by which microstructures may be intentionally made to have certain characteristics. We have explored a variety of manufacturing processes that allow for microstructure manipulation such as friction-stir welding, [70] heat treatment, and introducing voids into the material. While these processes may be utilized in many different ways, currently none of them can be used to consistently obtain designer selected values of material microstructures. We now explore a theory that allows one to consistently obtain desired microstructures and therefore desired material properties. The theory of rotations and laminations allows one to take any initial microstructure and create a new microstructure by stacking and welding metal layers – with directionally dependent material properties – at specific rotations. This theory, coupled with UC technology, allows the designer to hold the alloy fixed, yet modify material properties by choosing layer configuration and orientation.

Recall that the material property closure is the set of all material properties that are possible if one could create all possible microstructures. Since not all microstructures are practically obtainable, the achievable space in the property closure is limited. Implementation of the rotation and lamination theory, however, greatly expands the achievable space in the property closure as shown in Figure 6.4 for Ni 201 for example. The axes shown

in Figure 6.4 represent two different material properties: material compliance (elasticity) on the x-axis and yield strength on the y-axis. Note the subscripts, which represent desired directions for which the properties apply. The outermost loop, and the area it contains, represents every possible combination of these two properties. A single point represents a specific value for both the compliance and the yield strength which may be mapped to one or more microstructures that will have those properties. The triangle in Figure 6.4 represents isotropic material properties for Ni 201 while the star represents the starting microstructure of the material – as defined by OIM – in the direction of interest. The inner loop that traverses the star, and the area it contains, represents all properties that can be obtained by implementing the rotation and lamination theory to that starting microstructure when all rotations about the normal axis of the respective layer is considered. The remaining loop and the area it contains represents material properties that may be obtained by performing the rotation and lamination process twice (rank 2 lamination) to obtain even more complicated microstructures. It is important to note that any microstructure obtained by conventional methods, such as heavy rolling, can be greatly enhanced to obtain new microstructures and thus enabling new combinations of material properties that are typically thought to be unobtainable.

In this chapter we have presented theories and technologies that enable a designer to create products with a microstructure sensitive design. The microstructure sensitive design approach is beneficial for the designer for two principal reasons: (i) desired, even superior product performance often unobtainable by geometry modification is easily obtained with microstructure manipulation, and (ii) microstructure sensitive design results in a large barrier to those who would reverse engineer the products.

Chapter 7

Optimization Framework for Increasing the Barrier to Reverse Engineering Based on Microstructure Manipulation

In this chapter we provide a basic description of a generic framework in which one can obtain desired material properties in metals using common metal alloys. Specifically, this material manipulation process can be used to design products with a large barrier to reverse engineering as demonstrated by the case studies presented in Chapter 8. Figure 7.1 presents the framework and shows that four main phases comprise the process; Phase 0 – initialization of system parameter values, Phase 1 – gathering selected alloy data, Phase 2 – definition of feasible range of continuous material properties obtainable by rotations and laminations, and Phase 3 – material property exploration and selection using optimization techniques.

7.1 Phase 0 – Initialize Input Parameters

Let us first consider Phase 0. This part of the framework requires designer input which will then be used to determine fixed parameters and variables for the numerical optimization in Phase III. At this phase, the designer will select the material class, M, a specific alloy, M_0, from the chosen class to be used as the lamina material, and the number of lamina, N, to be used when creating the material with the desired properties. Importantly, the designer will select at least one direction of interest, w, x, y, z, and the desired material properties in the selected directions. Target material properties may include Young's modulus, E_t, yield strength, σ_{yt}, shear modulus, G_t, and Poisson's ratio, ν_t. The desired material properties may be the same or different values for different directions of interest. If a target value for a material property exceeds the range of feasible properties obtainable

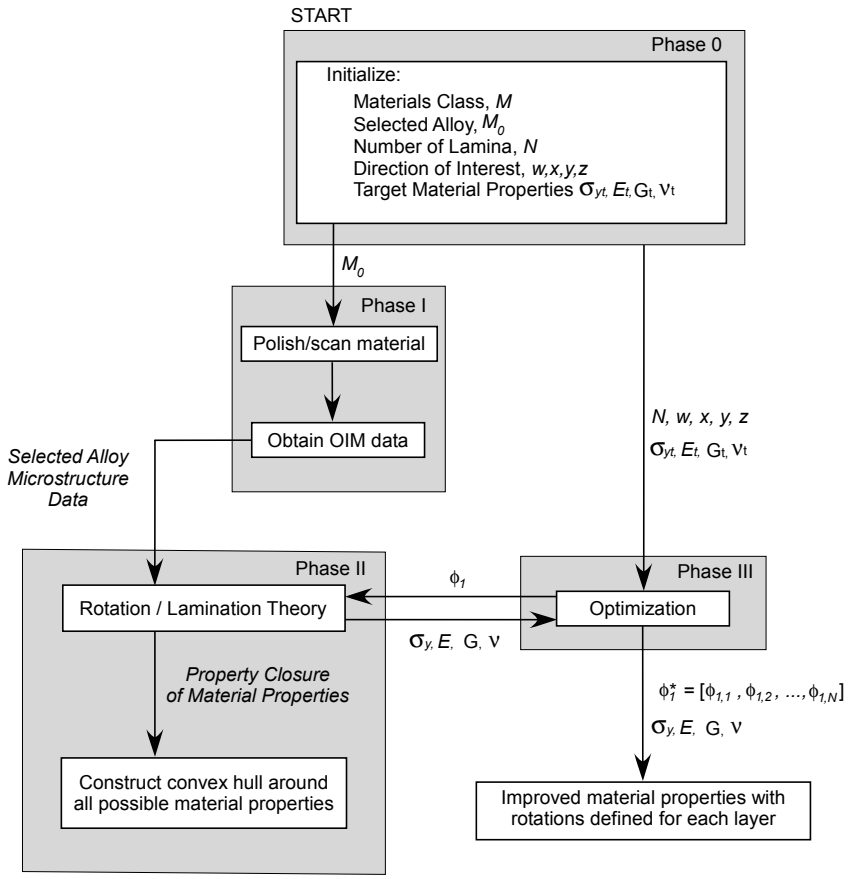

Figure 7.1: Flowchart of proposed framework to obtain improved material properties with common materials. As a note, Phase II is discussed in detail in Sections 6.3 and 6.4.

with the rotation/lamination theory, the optimization routine will obtain the properties closest to the target properties. The selected alloy will be analyzed in Phase I to generate the feasible range of material properties (generated in Phase II) that can be obtained with the rotation/lamination theory.

7.2 Phase I – Characterize Microstructure of Selected Alloy

Before one can obtain desired material properties in a material, one first needs to acquire microstructure information about that material. This is done by polishing and scanning the sample with a scanning electron microscope and analyzing the data with OIM software [55]. The data collected includes grain size, grain distribution, grain orientation

and other microstructure information specific to the sample. Once microstructure data is gathered, the range of material properties may be determined as described in Phase 2.

7.3 Phase II – Determine the Full Range of Material Properties Obtainable with Rotations and Laminations for the Selected Alloy

Different microstructures will result in different property closures. A material that is isotropic is unable to have a property closure larger than a single point since material properties are the same no matter how the sample is rotated. On the other hand, anisotropic materials made with a single crystal have the most directionally dependent material properties as the properties may change significantly even with a small rotation. The OIM data found in Phase 1 determines the microstructure of the selected alloy, thus determining the degree of anisotropy that exists in the sample. The OIM data is then used in the rotation/lamination theory – as described in detail in Sections 6.3 and 6.4 – to determine material properties in a given direction. When the rotation/lamination theory is applied for every orientation from $0 - 2\pi$ a complete property closure is created, which reveals the range of material properties that may be obtained with the sample-specific microstructure. When symmetry exists in the microstructure, the range of orientations required to obtain the complete property closure can be reduced. A convex hull encloses the resulting property closure and is principally used to help the designer know the feasible range of material properties for the given material. This is the process that was performed on Ni 201 to obtain the property closures in Figure 6.4.

7.4 Phase III – Determine Rotation/Lamination Strategy Required to Obtain Desired Material Properties for Selected Alloy

In this phase, we use an optimization routine to determine the manufacturing strategy – specifically the rotation of each layer – to create a laminated material with the desired material properties in the direction of interest. As input parameters, this optimization requires the number of laminations, N, the direction of interest, w, x, y, z, and the target values of the material properties of interest which are all determined by the designer in Phase 0. The optimization selects a value of ϕ_1 for each lamina and then determines the

effective material properties of the composite part (of N layers) in the direction of interest with the rotation/lamination theory (described in Phase 2). The process is repeated until the optimization determines the orientations required for each layer to obtain the desired material properties in the desired direction. Notice that for clarity we have expressed Young's modulus and yield strength as a function of ϕ_1.

The optimization problem statement, is formulated as follows:

$$\min_{\phi_1} \mu = w_1(\sigma_y(\phi_1) - \sigma_{yt})^2 + w_2(E(\phi_1) - E_t)^2 \tag{7.1}$$

subject to

$$0 \leq \phi_{1,i} \leq \pi \qquad \forall i = 1,2,...,N \tag{7.2}$$

where $\phi_1 = [\phi_{1,1}, \phi_{1,2}, ..., \phi_{1,N}]$ and represents the orientation of each layer, σ_{yt} is the desired value of yield strength, E_t is the desired value of Young's modulus, σ_y and E (which are both functions of $\phi_{1,i}$) are obtained from the microstructure-to-material-property process as described in previous chapters and in Figure 6.4, w_1 and w_2 appropriately scale the objectives, and Equation 7.2 is the upper and lower limits on the design variable. The solution of the optimization is the improved material properties E and σ_y – which are the material properties of the laminated part in the direction of interest – and the vector ϕ_1^* which is the required orientation of each layer. During the process of the optimization, the microstructure of each layer is oriented to obtain material properties for the part as close as possible to the desired properties. It is important to note that although the material properties of the individual layers may be different than the desired material properties, when the layers are combined at the orientations specified by the optimization, the overall effective properties of the layered material will closely match the desired material properties. This is true as long as the designer selected material properties that are contained within the property clo-

sure for that material. Now that the required rotation of each layer is known, the modified material, with the improved properties, may be created using the UC process.

In this chapter we have explored the optimization process. The optimization implemented the microstructure to material property theory to determine material properties for a part given an initial microstructure which resulted in the ideal rotation of N layers which will be used in the creation of the new material which will have the desired material properties. Importantly, the design framework presented in this chapter is key to designing, and manufacturing, products with the desired and unexpected performance ideal for impeding reverse engineering attempts.

Chapter 8

Increasing the Barrier to Reverse Engineering Case Studies

This chapter presents three case studies that demonstrate how microstructure sensitive design results in hardware with unexpected, yet desirable, mechanical performance. We reemphasize here that such designs can exhibit desirable behavior that is not intuitively understood, or easily replicated by examining the hardware in a reverse engineering setting. The first case study presents five cantilever-beam accelerometers with identical geometry and created from the same material but each accelerometer performs differently due to microstructure manipulation enabling the desired performance to be obtained. The second case study presents three bistable switches, each with a different microstructure, and explores the performance that can only be obtained with a heterogeneous microstructure. The third case study is an application of the reverse engineering relationships, as presented in this thesis, where the reverse engineering time and barrier is calculated and compared for a bistable switch with a homogeneous microstructure and a bistable switch with a heterogeneous microstructure. We show that by strategically manipulating the material microstructure, the barrier to reverse engineer a bistable switch nearly doubles while simultaneously achieving a superior performance. Table 8.1 presents the material property values that are used for the case studies presented.

8.1 Case Study 1: Cantilever-beam Accelerometer

The purpose of this case study is two fold: (i) to demonstrate the simple application of the presented developments for homogenously distributed material microstructures, and (ii) to demonstrate that parts of equal geometry, and equal material class and alloy, can provide different performance based on the orientation of anisotropic material.

Table 8.1: Material property values used for all calculations of Young's modulus and yield strength in the case studies. Note that K in this table represents the Hall-Petch slope.

Symbol	Value	Units
m	0.01	
$\dot{\gamma}_0$	0.001	1/s
D_0	0.001	
λ	1/2	
K	0.191	MPa*$\sqrt{m}$
$\overline{d}$	74.7	μm
τ_0	63.5	MPa
Nickel Material		
S_{11}	0.73	$\frac{10^{(-12)}*cm^2}{dyne}$
S_{12}	-0.27	$\frac{10^{(-12)}*cm^2}{dyne}$
S_{44}	0.8	$\frac{10^{(-12)}*cm^2}{dyne}$
Copper Material		
S_{11}	1.5	$\frac{10^{(-12)}*cm^2}{dyne}$
S_{12}	-0.63	$\frac{10^{(-12)}*cm^2}{dyne}$
S_{44}	1.3	$\frac{10^{(-12)}*cm^2}{dyne}$

8.1.1 Cantilever-beam Accelerometer Design Concept

Consider the design of a cantilever-beam accelerometer with a mass at the free end and an electrical circuit as seen in Figure 8.1. When acceleration is applied in the upward direction, the beam deflects downward and the mass comes in contact with the base, completing the circuit and sending an electrical signal indicating that a designer-specified acceleration has been reached. A total of five accelerometers are considered in this case study; all of them have identical geometry and are manufactured from the same stock material. Despite these critical similarities, each accelerometer can be designed to exhibit a unique force-deflection behavior. As shown shortly, the unique behaviors result from differences in material properties in the direction of the beam's long axis which are tailored through the rotation/lamination theory as presented in this thesis.

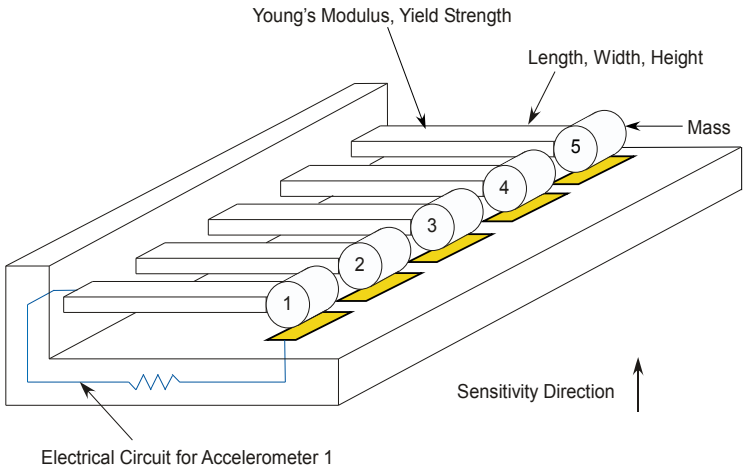

Figure 8.1: Simple array of cantilever-beam accelerometers with an electrical circuit that detects when the device has reached a prescribed acceleration.

8.1.2 Cantilever-beam Accelerometer Materials and Geometry

For this case study, the material considered is Ni 201 and the geometry is fixed according to the values in Table 8.2. The inital microstructure of the Ni 201 was obtained from OIM data after polishing and scanning samples of Ni 201. When designing under a common assumption of isotropic, homogeneous, linear-elastic materials, all five accelerometers exhibit the same force-deflection characteristic, thereby completing the electrical circuit at the same acceleration (5.17 m/s^2) as shown in Table 8.3. Alternatively, when designing to capitalize on material anisotropy, the rotation/lamination theory presented in this thesis enables designers to consistently obtain desired changes in material properties without changing geometry or material, thus achieving desired product performance. A few advantages of obtaining different performances with the same geometry and material are decreased tooling costs, potential barriers for competitors who may attempt to reverse engineer the product, and superior performance, such as withstanding more stress before failure, while maintaining product weight.

Table 8.2: Geometry for simple cantilever-beam accelerometers.

Constrained Accelerometer Geometry	
Length	10 mm
Width	2 mm
Height	1 mm
delta	1 mm
mass	0.02 kg

Table 8.3: Acceleration obtainable and respective Young's modulus for designing under isotropic, homogeneous assumptions.

Beam	Acceleration Required to Complete Circuit	Young's Modulus
1	5.17 m/s^2	206.8 GPa
2	5.17 m/s^2	206.8 GPa
3	5.17 m/s^2	206.8 GPa
4	5.17 m/s^2	206.8 GPa
5	5.17 m/s^2	206.8 GPa

8.1.3 Cantilever-beam Accelerometer Optimization and Construction

In order to perform the optimization and implement the rotation/lamination theory, we need to select a target acceleration for each accelerometer. We have selected five different target accelerations to be measured by the geometrically identical cantilever-beam accelerometers, which may be seen in Table 8.4, with the associated Young's modulus that will result in the desired performance.

Only now that we have the material and geometry selected, and the target accelerations known, can we run the optimization routine that determines how each layer needs to be oriented to obtain the desired value of Young's modulus resulting in the desired performance. The optimization problem statement for the cantilever beam accelerometers is given by Equations 8.1–8.3.

$$\min_{\phi_1} \mu = (E(\phi_1) - E_t)^2 \tag{8.1}$$

subject to

$$0 \leq \phi_{1,i} \leq \pi \qquad \forall i = 1,2,...,N \tag{8.2}$$

$$\sigma_{max} \leq \sigma_y(\phi_1) \tag{8.3}$$

where $\phi_1 = [\phi_{1,1}, \phi_{1,2}, ..., \phi_{1,N}]$ and represents the orientation of each layer, E_t is the desired value of Young's modulus, $\sigma_y(\phi_1)$ and $E(\phi_1)$ are obtained from the microstructure-to-material-property process as discussed previously, Equation 8.2 is the upper and lower limits on the design variable, and Equation 8.3 ensures that the cantilever beam does not yield under the loading conditions.

As the theory is valid for any number of layers, we consider the simplest case of one lamina, for illustration purposes. Similar to carbon-fiber composites, layering is important to obtain the desired thickness of a part. During the process of obtaining a strong initial microstructure – which expands the feasible range of material properties– the metal becomes very thin. If one desires a part thicker than the strong-textured metal, layering becomes necessary. Using UC for the welding process is desirable because of its excellent linear weld density and minimal affect on the grains surrounding the weld areas.

Table 8.4: Target accelerations for simple cantilever-beam accelerometers and respective value of Young's modulus required to obtain the acceleration with the fixed geometry and material alloy.

Beam	**Acceleration Required to Complete Circuit**	**Young's Modulus**
1	5.00 m/s^2	200.0 GPa
2	5.05 m/s^2	202.0 GPa
3	5.10 m/s^2	204.0 GPa
4	5.15 m/s^2	206.0 GPa
5	5.20 m/s^2	208.0 GPa

Table 8.5: Optimization results for five cantilever-beam accelerometers with fixed material alloy and geometry. Each beam has a unique acceleration which precisely correlates to the desired acceleration.

Beam	Acceleration Required to Complete Circuit	Young's Modulus	Orientation
1	5.00 m/s^2	200.0 GPa	106.39 Degrees
2	5.05 m/s^2	202.0 GPa	122.53 Degrees
3	5.10 m/s^2	204.0 GPa	148.40 Degrees
4	5.15 m/s^2	206.0 GPa	46.750 Degrees
5	5.20 m/s^2	208.0 GPa	38.850 Degrees

8.1.4 Cantilever-beam Accelerometer Design Results

The optimization routine, as described in Section 7.4, results in the orientation of the layers required to obtain the desired performance as well as the Young's modulus and yield strength of the composite material if aligned by the orientations defined by the optimization. Since there are five different beams, each with a unique desired acceleration, five separate optimizations are required. The results of the optimizations for this case study are shown in Table 8.5.

These results, which are obtained using only a mildly anisotropic material, lend insight into the kinds of performance differences one can achieve through simple single layer rotations. The effect is more dramatic with more anisotropic materials and higher order layering.

8.2 Case Study 2: Bistable Electronic Switch

The primary purpose of this case study is to demonstrate how unexpected mechanical performance can be obtained with strongly textured materials – even performances that are not obtainable with isotropic or anisotropic homogeneous materials. A secondary purpose of this case study is to reiterate that parts of identical geometry, and material class and alloy can be designed to have unexpected desirable performance, which would be difficult to discern in a reverse engineering setting.

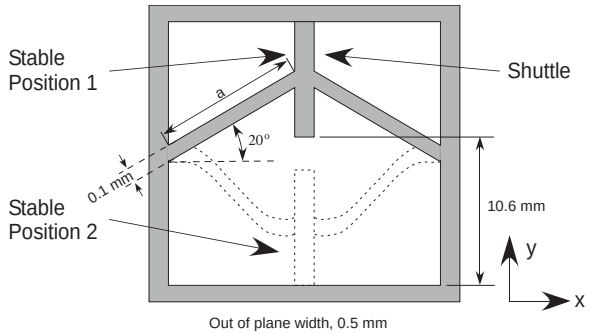

Figure 8.2: A compliant bistable switch with the two equilibrium positions of the shuttle shown. Not drawn to scale.

8.2.1 Bistable Electronic Switch Design Concept

A bistable mechanism is a device that tends toward one of two stable equilibrium positions. A *compliant* bistable mechanism achieves its motion by deflecting its compliant members, and by so doing the energy required to hold the mechanism in either of its equilibrium positions is stored in the form of strain energy [71, 72]. Figure 8.2 shows the basic concept for a compliant bistable switch, which is composed of a shuttle that travels in the y-direction by the flexing of its two arms. The gray region indicates the part and the white region is void of material. The shuttle will tend toward one of the two positions shown in Figure 8.2. The mechanism can be used as an electronic switch when the shuttle and frame are part of an electrical circuit; when the shuttle contacts the frame, as in Stable Position 1, the circuit is complete.

8.2.2 Bistable Electronic Switch Materials and Geometry

In this case study, we consider three bistable switches, all of which have identical geometry and are created with the same phosphor bronze copper – a material commonly used for electrical connectors in the connector industry. A single crystal of phosphor bronze is used for the bistable electronic switch presented in this case study. A numerical approximation of the single crystal material microstructure is used to predict the material properties of yield strength and Young's modulus. One of the three bistable switches considered is designed under the assumption that the phosphor bronze copper is isotopic, linear-elastic,

and homogeneous – an assumption commonly used in the electrical connector industry. The second bistable switch is designed under the assumption that the material is anisotropic and homogeneous, while the last switch material is designed by considering material anisotropy and heterogeneity. Both anisotropic cases use the rotation/lamination theory presented in this thesis to identify designs with unexpected, yet desirable, mechanical performance.

8.2.3 Bistable Electronic Switch Optimization and Construction

The reason for considering three bistable switches is to see if, through the developments presented herein, we can identify a switch geometry that would meet the design requirements *only* when an anisotropic, *heterogeneous* design approach is used. That is, for the same geometry, and same material class and alloy, the *homogeneous* cases would simply not meet the requirements. To identify such a design we use a numerical optimization routine.

We pause briefly to note that the process of finding a design that does not work when common design assumptions are made is beneficial for preventing competitors from reverse engineering a product. Assuming a competitor could match the material and geometry identically, the copied product will not have the required performance thus impeding the competitor from easily recreating the original product for their own use.

For the bistable switches, the optimization routine used seeks to minimize the length of the compliant arms, a, and simultaneously reach a target force (F_t) the switch is able to exert in the deflected position. Other geometric features are fixed according to the values seen in Figure 8.2. More formally, the optimization problem statement is given by Equations 8.4–8.8.

$$\min_{a,\phi_1} \mu = w_3 W(a) - w_4 (F(a,\phi_1) + (-F_t/(N_a)))^2; \tag{8.4}$$

subject to

$$10\text{mm} \leq a \leq 50\text{mm} \tag{8.5}$$

$$0 \leq \phi_1 \leq \pi \tag{8.6}$$

$$F(a, \phi_1) < 0 \tag{8.7}$$

$$\sigma_{max} \leq \sigma_y(\phi_1) \tag{8.8}$$

where W is the total width of the bistable switch, F is the force output of a single arm in the deflected position, N_a is the number of arms on the bistable switch, a is the length of the compliant arms, w_3 and w_4 appropriately scale the objectives, and σ_{max} is the maximum stress the compliant beams experiences throughout the entire path of motion. The relationship imposed by Equation 8.7 ensures bistability [72]. Here we note that each arm is individually optimized.

Recall that in Phase 0 of Section 7.1 the designer selects a direction of interest and target material properties. The optimization routine described in Phase 3 in Section 7.4 then searches for designs that match the material properties in the direction of interest to the target material properties specified by the designer. The direction of interest for *a single arm* of the bistable switch is the direction parallel to the arm. The force output of that single arm is given according to Equation 8.9 where α is a the non-dimensional force [72].

$$F(a, \phi_1) = \frac{\alpha^2 E(\phi_1) I}{a^2} \tag{8.9}$$

As illustrated by Equation 8.9 the force, F, is directly proportional to Young's modulus in the direction of interest. For the full mathematical development of a fully-compliant bistable switch see Todd [72]. For single crystal materials, the largest value of Young's modulus is parallel to the crystal's texture and the smallest value of Young's modulus is perpendicular to the texture direction. Therefore, in order to reach relatively small target force values using a bistable switch, the single crystal texture must be aligned perpendicular to the shuttle arms.

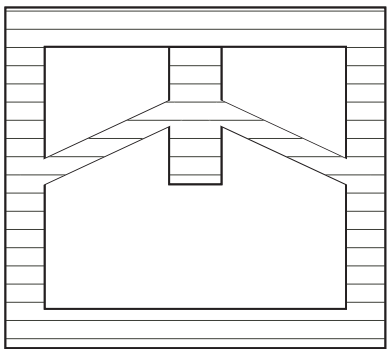

Figure 8.3: A compliant bistable switch with anisotropic homogeneous material properties. Texture direction denoted by hatching.

If the mechanism arms could be treated independently, the same design, optimization, and construction approach used in Case Study 1, could be used. Because of their orientation, it is impossible to select a single crystal orientation that is parallel or perpendicular to both arms simultaneously – if a homogeneous material is used. We therefore consider a heterogeneously distributed microstructure, which is illustrated by the hatching in Figure 8.5.

To construct the heterogeneous material, a rolling and Friction Stir Welding [70] (FSW) process is used. Figure 8.4 illustrates the process; the original copper material is first rolled to create a large degree of anisotropy in the material texture; next, two triangles are cut out of the copper. The complimentary triangles are then joined together using FSW. While any metal joining process could be used to join the separate copper pieces, FSW is used in this case study, because after cleaning and polishing, the FSW joint is nearly impossible to detect without use of a scanning electron microscope, therefore making the heterogeneous nature of the microstructure difficult for competitors to detect. Figure 8.5 shows how the compliant bistable switch is cut from the heterogeneous sheet.

8.2.4 Bistable Electronic Switch Design Results

Table 8.6 compares the results of the design optimization. All three switches have identical geometry, and are constructed using the same stock material. Notice that the isotropic material resulted in a force that exceeds the target force by 80.6%. For electri-

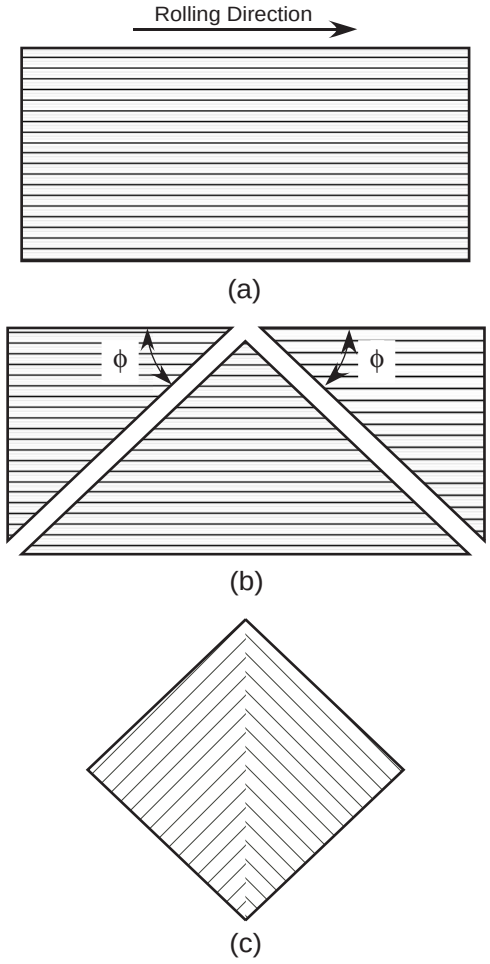

Figure 8.4: Process by which heterogeneous material properties may be created to obtain unexpected performance from original material. Texture direction denoted by hatching.

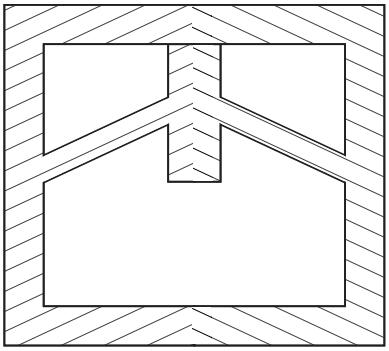

Figure 8.5: A compliant bistable switch cut from a sheet that is anisotropic and heterogeneously symmetric about the mid-plane. Texture direction denoted by hatching.

Table 8.6: Optimization results for three bistable switches made with identical geometry and with phosphor bronze copper. The symbol β represents the angle of the compliant arms of the bistable switch from the horizontal plane.

Fixed Parameters for all three switches [54]			**Heterogeneous, Anisotropic Material**			**Homogeneous, Anisotropic Material**			**Isotropic Material [54]**		
a	23.31	mm	E	66.67	GPa	E	83.52	GPa	E	120.7	GPa
F_t	1.2	N	F	1.211	N	F	1.513	N	F	2.1866	N
σ_y	552	Mpa	SF	1.23		SF	0.97		SF	0.67	
β	20	degrees									
N_a	2										

cal connectors, excessive force results in excessive wear and reduces the performance life of the connector. Additionally, the anisotropic homogeneous approach also exceeded the target force by 24.9%, while the anisotropic heterogeneous approach is very close to the target force. When a comparison of the safety factors is conducted, one can see that only the anisotropic heterogeneous material did not fail while the homogeneous, anisotropic material and the isotropic materials both failed with a safety factor (SF) being less than one. The value of yield strength used for this case study was obtained from literature [54] and assumed to be the same in all directions. While the mathematical model is in place, there was not sufficient data for the single crystal copper material to accurately predict yield strength with respect to sample orientation. Future efforts will focus on obtaining single crystal copper information required to predict yield strength as a function of sample orientation. We can conclude, therefore, that through a microstructure sensitive design approach, coupled with numerical optimization, designs with unexpected desirable performance can be identified, and can be made difficult to reverse engineer.

8.3 Case Study 3: Time and Barrier Analysis of a Bistable Mechanism

In this section, we use the metrics and parameters defined in Chapter 4 to determine the time and barrier to reverse engineer the bistable switch as described in Section 8.2. Let us take the perspective of the original designer reverse engineering the bistable switch with the homogenous microstructure for this example. The only design constraint for this example is to prevent yielding of the flexible members as the mechanism travels through

the entire range of motion. We are interested in knowing the barrier and time to reverse engineer the device. Specifically, we consider two information types, linear geometric information and material microstructure information.

To determine the time and barrier to reverse engineer this bistable mechanism, we start by determining the values of the parameters K_i, F_i, and P_i, for each information type i. When K_i, F_i, and P_i are known for each i, we calculate the barrier, B_i, and time, T_i, for each information type individually. With B_i and T_i known, the total barrier, B^*, of the product and the total time, T^*, to reverse engineer the product can be determined.

8.3.1 Geometry Analysis of a Bistable Mechanism

In this section, we describe the quantification of K_g, F_g, and P_g for the bistable mechanism where the subscript g represents *linear geometric information*. We start by discussing K_g.

While a total of nine linear dimensions are required to describe the geometry of the product, only eight dimensions are critical to performance since stress is not affected by out of plane thickness and, for this example, there is no constraint on the output force. As a note, an analysis of the governing equations for Euler beams with a prescribed deflection show the out-of-plane thickness has no effect on the bending stress experienced by the beam. When competitors reverse engineer the bistable mechanism, it may not be obvious that the out-of-plane thickness of the device is not critical for performance, therefore an appropriate selection of $K_g(\tau_0)$ is nine as all nine dimensions are likely to be extracted. An important observation to make is that whenever $K_g(\tau)$ is larger than $K_g(t)$, the competitor is likely to extract more information than needed, thereby increasing the time to reverse engineer the product. With eight dimensions critical to performance, the value of $K_g(t_0)$ is eight recalling that $K_g(t_0)$ represents the quantity of pertinent information initially contained by the product. As shown in Table 8.7, $K_g(t_0)$ is 8 and $K_g(\tau_0)$ is 9.

The value of F_g is the rate at which the competitors can extract geometric information. Since it is difficult, if not impossible, to determine the rate at which competitors can extract geometric information, a close approximation is to determine the rate at which one's own company can extract geometric information. One method to determine F_g is to

Table 8.7: Parameters and metrics determined for geometric information of a homogeneous bistable mechanism. Time is in seconds.

Description	Parameter	Value
Initial *pertinent* geometric information contained by product.	$K_g(t_0)$	8
Initial geometric information contained by product.	$K_g(\tau_0)$	9
Initial geometric extraction rate.	$F_g(\tau_0)$	0.057
Initial power exerted to extract geometric information.	$P_g(\tau_0)$	1
Description	**Metrics**	**Value**
Geometric information storage ability.	S_g	0.513
Barrier to extracting geometric information.	B_g	307.8
Estimated time to extract geometric information.	T_g	473

simply measure the rate at which dimensions can be extracted. Importantly we note that when the flow rate for one information type is determined, that flow rate may be used in the analysis of other products that contain that same information type. Through experimentation, the initial flow rate of linear dimensions, for the original designer, has been discovered to be approximately 0.057 dimensions per second. The flow rate of pertinent information is likely to vary from designer to designer depending upon resources and skills available. Therefore, $F_g(\tau_0)$ is quantified as 0.057 as shown in Table 8.7.

Power is the measure of the effort being exerted per time by the competitor reverse engineering the product. While there may be reason to set P to be less than one, for this example, P_i is assumed to always be equal to one for all information types. This implies that competitors are exerting their best effort to extract information from the bistable mechanism, which is the most conservative approach.

The calculation of S_g is carried out by Eq. 4.4 enabling the calculation of B_g and T_g with Eqs. 4.1 and 4.5, respectively. The barrier to extract geometric information is 307.8 and the estimated time to extract geometric information is 473 seconds. Table 8.7 presents the parameters and metrics defined in this section.

8.3.2 Microstructure Analysis of a Bistable Mechanism

In this section, we describe how K_m, F_m, and P_m are quantified for the bistable mechanism with the homogeneous microstructure, where the subscript m represents *material microstructure information*. Based on the quantified parameters, we also calculate B_m and T_m. There are many ways to characterize material microstructures including measuring the orientation of each grain and modeling orientation distribution through Fourier series. Each method of characterizing the microstructure can effectively be used to determine B_m and T_m as long as the flow rate of information extraction can be determined. For this example, we assume that an entire microstructure is a single piece of information and the extraction rate of microstructure information can be determined. We also assume that the competitors are as skilled as the original designers in understanding and analyzing material microstructures. For this reason, a good approximation of F_m may be to measure the rate of microstructure information extraction of the original designers.

For this example, the microstructure extraction rate is chosen to be one microstructure in ten hours or a flow rate of $2.778 * 10^{-5}$ seconds – which includes sample preparation (such as polishing and mounting sample), scanning the sample with a scanning electron microscope, and data analysis with Orientation Image Microscopy software. We note that this flow rate is based on the authors' own experience in microstructure information extraction. If the microstructure of the bistable mechanism is a homogeneous microstructure, it is likely that the microstructure can be determined correctly without extracting excess information. This implies that $K_m(\tau_0)$ is 1 and $K_m(t_0)$ is also 1. As was mentioned in Section 8.3.1, P_m is also 1. With K_m, F_m, and P_m defined, S_m, B_m, and T_m are calculated with numerical results presented in Table 8.8. It can be seen, based on the table, that extracting microstructure information requires significantly more time when compared to linear geometric information. Therefore designers who wish to protect innovative designs can find more effective barriers to reverse engineering in the microstructure of the material when compared to geometry.

Table 8.8: Parameters and metrics determined for microstructure information of a homogeneous bistable mechanism. Time is in seconds.

Description	Parameter	Value
Initial *pertinent* microstructure information contained by product.	$K_m(t_0)$	1
Initial microstructure information contained by product.	$K_m(\tau_0)$	1
Initial microstructure extraction rate.	$F_m(\tau_0)$	$2.778 * 10^{-5}$
Initial power exerted to extract microstructure information.	$P_m(\tau_0)$	1
Description	**Metrics**	**Value**
Microstructure information storage ability.	S_m	$2.778 * 10^{-5}$
Barrier to extracting microstructure information.	B_m	$1.3 * 10^{9}$
Estimated time to extract microstructure information.	T_m	$1.080 * 10^{5}$

8.3.3 Total Barrier and Time Calculation of a Bistable Mechanism

In the previous sections, the time and barrier to reverse engineer the homogeneous bistable mechanism was determined for each information type of interest. Following the developments of Section 4.3, the total barrier, B^*, and total time, T^*, to reverse engineer the bistable product as a whole is calculated and presented in Table 8.9.

Importantly, we note that the calculation of B^* does not adhere to Ohm's law; this is because each information type, in this case g and m, is treated independently. In the context of electrical circuits, each information type is an independent resistor-capacitor circuit. When the total barrier, B^*, for the product is calculated, a pseudo product is created with a quantity of pertinent information equivalent to the sum of pertinent information contained by the product for each individual information type; and the equivalent time required to extract that pertinent information. The total barrier is then calculated from this pseudo product. This enables products to be characterized with a single value that represents the overall barrier and time to reverse engineer the products.

To calculate T^*, K^*, and S^* we evaluate the summation of each T_i, K_i, and S_i respectively according to Eqs. 4.7, 4.8, and 4.9. Now F^* and P^* can be calculated according

Table 8.9: Parameters and metrics determined for all information of a homogeneous bistable mechanism. Time is in seconds.

Description	Metric	Value
All *pertinent* information initially contained by product.	$K^*(t_0)$	9
Information storage ability for all information types.	S^*	0.513
Estimated time to extract all information.	T^*	$1.085 * 10^5$
Initial extraction rate of all information.	$F^*(t_0)$	$8.31 * 10^{-5}$
Initial power exerted to extract all information.	$P^*(t_0)$	$1.46 * 10^{-3}$
Barrier to extracting all information.	B^*	$2.11 * 10^5$

to Eqs. 4.10 and 4.11, respectively. Finally, B^* can be calculated using Eq. 4.1 and using the values of P^* and F^* with results seen in Table 8.9.

The significance of these relationships is that they enable a systematic and consistent comparison of products. This product comparison can be used by companies to determine which products will yield the greatest return on investment when performing reverse engineering activities. Adversely, companies releasing a new product can estimate the time for competitors to reverse engineer the design. These relationships also supply information that enables minimal profit loss due to competition by understanding and implementing characteristics that make products difficult and time consuming to reverse engineer. The systematic estimation of the time required to reverse engineer a product also facilitates management decisions such as project costs and timelines. The nature of the relationships enables designers to use them in a numerical optimization routine to develop new designs that (i) meet or exceed desired performance, (ii) minimize costs, and (iii) maximize the time and barrier of reverse engineering. In the following section, we discuss how analysis of the relationships enabled the design of the bistable switch with a heterogeneous microstructure which has a superior performance, and is substantially more difficult to reverse engineer.

8.3.4 Making the Bistable Mechanism More Difficult to Reverse Engineer

As described in detail in Chapter 6, superior, even unexpected, performance can be achieved for the bistable mechanism when a multidisciplinary design approach is used. Specifically, when geometry *and* material microstructure are simultaneously considered, products that are intrinsically difficult to reverse engineer can be more easily designed. This section briefly describes how the barrier and time to reverse engineer a product can be increased by this multidisciplinary approach.

By analyzing the fundamental relationships for a bistable mechanism [71], it can be seen that when desirable microstructures are aligned along the length of each beam, superior compliance, and therefore performance, can be achieved with the process presented in Chapter 8 resulting in a bistable switch with a heterogeneous microstructure. As shown in this chapter, the heterogeneous microstructure substantially increases the time and barrier to reverse engineer the mechanism. Even if the competitor can create an imitation of the bistable mechanism with identical geometric features and material alloy, the imitated device will not match the performance of the original design with the heterogeneous microstructure.

Table 8.10: Parameters and metrics determined for all information of a bistable mechanism with a heterogeneous material microstructure. Time is in seconds.

Description	Metric	Value
All *pertinent* information initially contained by product	$K^*(t_0)$	10
Information storage ability for all information types	S^*	0.513
Estimated time to extract all information	T^*	$2.165 * 10^5$
Initial extraction rate of all information	$F^*(t_0)$	$4.631 * 10^{-5}$
Initial power exerted to extract all information	$P^*(t_0)$	$9.02 * 10^{-4}$
Barrier to extracting all information	B^*	$4.21 * 10^5$

Assuming a competitor determines that the product was created with a heterogeneous microstructure approach, there still exist multiple barriers to overcome before the product can be truly reverse engineered. Namely, (i) how many microstructures exist in the product, (ii) which microstructures are critical to performance, (iii) how to obtain desired microstructure, and (iv) how to seamlessly join multiple parts. As can be seen in Table 8.10, the total time and barrier to reverse engineer a bistable mechanism with a heterogeneous microstructure is notably greater than the bistable mechanism with a homogenous microstructure. A simple, yet important, observation to make is that it would have been possible for the designer to make the geometry of the mechanism more difficult to reverse engineer, but due to the different rates of information extraction for geometric and microstructure information this would have had minimal effect on the total time and barrier.

Chapter 9

Concluding Remarks

In this thesis, we have presented general metrics for evaluating the barrier and time to reverse engineer a product. We have also defined supporting metrics and parameters for evaluating the barrier and time with an average error of 12.2%. The metrics and parameters presented are adapted from Ohm's Law and are based on resistor-capacitor circuits and capacitor discharge time estimates.

We have also presented an approach that uses material microstructure information, numerical optimization, and state-of-the-art manufacturing techniques to create designs with unexpected desirable performance that are difficult to reverse engineer – a powerful combination for companies who wish to make innovative products and devices available to the masses without disclosing the phenomena that gives the device its unexpected performance. The root of the method is in manipulating the material microstructure, while constrained to existing manufacturing methods (rolling, UC, and FSW). The consideration of these manufacturing approaches is embodied in the rotation/lamination theory and in the minimal negative affect that these joining processes have on the microstructures of interest. Two simple case studies were presented that illustrate the basic benefits that come from the presented design approach. The first case study used actual microstructure data and showed how performance can be varied in geometrically identical products made from the same stock material by tailoring the material properties, in directions of interest, with the rotation/lamination theory presented in this thesis. The second case study explored the application of heterogeneous, anisotropic microstructures that enable a performance not obtainable with isotropic or homogeneous material properties. The third case study utilizes the reverse engineering metrics presented in this thesis to calculate the time and barrier

to reverse engineer a bistable switch with a homogeneous microstructure and a bistable switch with a heterogeneous microstructure. We can, therefore, see from the case studies that through a microstructure sensitive design approach, coupled with numerical optimization, enables manufacturable designs with superior performance while simultaneously increasing the barrier to reverse engineer the product.

From a design point of view, the developed metrics can be used to compare one design versus another, where the barrier and time to reverse engineering can be quantified. Metrics for evaluating the time and barrier to reverse engineer a product enables the original designer to strategically identify and improve product characteristics so as to increase the difficulty and time to reverse engineer them. To competitors reverse engineering the original designs, minimal time and barrier is desired so as to enter the market before it is saturated. The developed metrics can, therefore, be used to assist competitors to focus on products that can be reverse engineered sufficiently fast. Additionally, they can be used to help competitors see how to improve its reverse engineering capabilities.

Ongoing and future developments include exploration of additional microstructure manipulation strategies, and the optimization of products with the new and additional objective of increasing the time and/or barrier to reverse engineer a product. Uncertainty analysis will also be conducted which will determine the variation of the actual barrier to reverse engineering when products are modified to be more difficult to reverse engineer. We reiterate here, that the total time, T^*, and total barrier, B^*, is the time and barrier to only extract information from a product. Future developments will include the time and barrier to imitate and fabricate the product which will also include analysis of development cost and return on investment.

References

[1] Harston, S. P., Mattson, C. A., Adams, B. L., and Ahmadi, S., 2008. "Capitalizing on heterogeneity and anisotropy to find designs with unexpected performance." In *12th AIAA/ISSMO Multidisciplinary Analysis and Optimization Conference, Victoria, British Columbia, Canada, AIAA 2008-6015*.

[2] Ingle, K. A., 1994. *Reverse Engineering*. McGraw-Hill, New York, NY.

[3] Otto, K., and Wood, K., 2001. *Product Design*. Prentice Hall, Upper Saddle River, NJ.

[4] Koeppel, D., 2007. "China's iclone." *Popular Science*, http://www.popsci.com/iclone.

[5] Samuelson, P., and Scotchmer, S., 2002. "The law and economics of reverse engineering." *The Yale Law Journal,* **111**(7), pp. 1575–1663.

[6] Roberts, D., 2005. "Did spark spark a copycat." *BusinessWeek*, http://www.businessweek.com/magazine/content/05_06/b3919010_mz001.htm

[7] CNN, 2001. "How soviets copied america's best bomber during wwii." *CNN*, http://archives.cnn.com/2001/US/01/25/smithsonian.cold.war/.

[8] Macmillan, I., McCaffery, M. L., and van Wijk, G., 1985. "Competitors' responses to easily imitated new products-exploring commercial banking product introductions." *Strategic Management Journal,* **Vol. 6, No. 1**, pp. 75–86

[9] Mansfield, E., Schwartz, M., and Wagner, S., 1981. "Imitation costs and patents: An empirical study." *The Economic Journal,* **Vol. 91, No. 364**, pp. 907–918.

[10] Chikofsky, E. J., and Cross, J. H., 1990. "Reverse engineering and design recovery: a taxonomy." *Software, IEEE,* **7**, pp. 13–17.

[11] Csete, M., and Doyle, J., 2002. "Reverse engineering of biological complexity." *Science,* **295**, pp. 1664–1669.

[12] Waters, R., and Chikofsky, E., 1994. "Reverse engineering: progress along many dimensions." *Communications of the ACM,* **37**, pp. 22–25.

[13] Buss, E., De, R., Gentleman, M. M., Henshaw, J., Johnson, H., Kontogiannis, K., Merlo, E., Muller, H., Mylopoulos, J., Paul, S., Prakash, A., Stanley, M., Tilley, S., Troster, J., and Wong, K., 1994. "Investigating reverse engineering technologies for the CAS program understanding project." *IBM Systems Journal,* **33**, pp. 477–500.

[14] Nelson, M. L., 1996. "A survey of reverse engineering and program comprehension." http://www.citebase.org/abstract?id=oai:arXiv.org:cs/0503068.

[15] Muller, H. A., Jahnke, J. H., Smith, D. B., Storey, M.-A. D., Tilley, S. R., and Wong, K., 2000. "Reverse engineering: A roadmap." In *Proceedings of the International Conference on Software Engineering (ICSE)*.

[16] Reed, R., and DeFillippi, R. J., 1990. "Casual ambiguity, barriers to imitation, and sustainable competitive advantage." *The Academy of Management Review,* **15**, p. 88.

[17] Pahl, G., Beitz, W., Feldhusen, J., and Grote, K.-H., 2007. *Engineering Design: A Systematic Approach*. Springer, Verlag, London.

[18] Moles, C., Mendes, P., and Banga, J., 2003. "Parameter estimation in biochemical pathways: a comparison of global optimization methods." *Genome Research,* **13**, pp. 2467–2474.

[19] Kremling, A., Fischer, S., Gadkar, K., Doyle, F. J., Sauter, T., Bullinger, E., Allgwer, F., and Gilles, E. D., 2004. "A benchmark for methods in reverse engineering and model discrimination: Problem formulation and solutions." *Genome Research,* **14**, pp. 1773–1785.

[20] Benyus, J. M., 2002. *Biomimicry: Innovation Inspired by Nature*. HarperCollins Publishers Inc., New York, NY.

[21] Naumovich, G., and Memon, N., 2003. "Preventing piracy, reverse engineering, and tampering." *Computer,* **36**, pp. 64–71.

[22] Besl, P. J., and Mckay, N. D., 1992. "A method for registration of 3-d shapes." *IEEE Transactions on Pattern Analysis and Machine Intelligence,* **14**(2), February, pp. 239–256.

[23] Vrady, T., Martin, R. R., and Cox, J., 1997. "Reverse engineering of geometric models: An introduction." *ComputerAided Design,* **29**, pp. 255–268.

[24] Myers, R. H., Montgomery, D. C., and Anderson-Cook, C. M., 2009. *Response Surface Methodology: Process and Product Optimization Using Designed Experiments (Wiley Series in Probability and Statistics)*., 3 ed. Wiley, New York, NY, January.

[25] Simpson, T., Poplinski, J., Koch, P., and Allen, J., 2001. "Metamodels for computer-based engineering design: Survey and recommendations." *Engineering with Computers,* **17**, pp. 129–150.

[26] Scherer, F. M., 1967. "Research and development resource allocation under rivalry." *Quarterly Journal of Economics,* **81**, pp. 359–94.

[27] Mansfield, E., Rapoport, J., Romeo, A., Villani, E., Wagner, S., and Husic, F., 1977. *The Production and Application of New Industrial Technology*. W. W. Norton.

[28] Shapiro, C., 1985. "Patent licensing and r & d rivalry." *American Economic Review,* **75**, pp. 25–30.

[29] Nelson, R., and Winter, S., 1982. *An evolutionary theory of economic change*. Belknap Press, Cambridge, Massachusetts.

[30] Hill, C. W. L., 1992. "Strategies for exploring technological innovations: When and when not to license." *Organization Science,* **3**, pp. 428–441.

[31] McEvily, S. K., and Chakaravarthy, B., 2002. "The persistance of knowledge-based advantage: An emperical test for product performance and technological knowledge." *Strategic Management Journal,* **23**, pp. 285–305.

[32] Afshar, M. H., 2008. "Layout and size optimization of tree-like pipe networks by incremental solution building ants." *Canadian Journal of Civil Engineering,* **35**, pp. 129–139.

[33] Lassila, T., 2009. "Optimal damping of a membrane and topological shape optimization." *Structural and multidisciplinary optimization,* **38**, pp. 43–52.

[34] Tavakoli, R., and Davami, P., 2009. "Optimal riser design in sand casting process with evolutionary topology optimization." *Structural and multidisciplinary optimization,* **38**, pp. 205–214.

[35] Nelson, S. A., Parkinson, M. B., and Papalambros, P. Y., 2001. "Multicriteria optimization in product platform design." *Journal of mechanical design,* **123**, pp. 199–204.

[36] Hariharan, K., and Balaji, C., 2009. "Material optimization: A case study using sheet metal-forming analysis." *Journal of Materials Processing Technology,* **209 Issue 1**, pp. 324–331.

[37] Xia, Q., and Wang, M. Y., 2008. "Simultaneous optimization of the material properties and the topology of functionally graded structures." *Computer-Aided Design,* **40**, pp. 660–675.

[38] Chen, B. S., and Tong, L. Y., 2005. "Thermomechanically coupled sensitivity analysis and design optimization of functionally graded materials.." *Computer Methods in Applied Mechanics and Engineering,* **194**, pp. 1891–1911.

[39] Adams, B. L., Nylander, C., Aydelotte, B., Ahmadi, S., Landon, C., Stucker, B. E., and Janaki-Ram, G. D., 2008. "Accessing the elastic-plastic properties closure by rotation and lamination." *Acta materialia,* **56**, pp. 128 –139.

[40] White, D., 2003. "Ultrasonic consolidation of aluminum tooling." *Advanced Materials and Processes,* **161**, pp. 64–65.

[41] Messac, A., and Mattson, C. A., 2004. "Normal constraint method with guarantee of even representation of complete pareto frontier." *AIAA Journal,* **42**(10), pp. 2101–2111.

[42] Messac, A., and Mattson, C. A., 2005. "Pareto frontier based concept selection under uncertainty, with visualization, optimization and engineering." *Kluwer Publishers - Special Issue on Multidisciplinary Design Optimization, Invited Paper,* **6**(1), pp. 85–115.

[43] Mattson, C. A., Mullur, A. A., and Messac, A., 2004. "Smart pareto filter: Obtaining a minimal representation of multiobjective design space, engineering optimization." *Engineering Optimization,* **36**(4), pp. 721–740.

[44] Ohm, G. S., 1827. *Die galvanische Kette, mathematisch bearbeitet*. Berlin, Germany.

[45] Akers, A., 2006. *Hydraulic Power System Analysis*. Taylor & Francis, Boca Raton, FL

[46] Chernov, I. N., Eyink, L., Lebowitz, J. L., and Sinai, Y. G., 1993. "Derivation of ohm's law in a deterministic mechanical model." *Physical review letters,* **70**, pp. 2209–2212

[47] Jiles, D., 2001. *Introduction to the Electronic Properties of Materials*. CRC Press, Boca Raton, FL

[48] Dorf, R. C., 1993. *The Electrical Engineering Handbook*. CRC Press, Boca Raton, FL.

[49] Rizzoni, G., 2004. *Principles and Applications of Electrical Engineering*. McGraw-Hill, New York, NY.

[50] Hartley, R. V. L., 1928. "Transmission of information." *Bell System Technical Journal*, p. 535.

[51] Shannon, C. E., 1948. "A mathematical theory of communication." *The Bell System Technical Journal,* **27**, pp. 379–423.

[52] von Hippel, E., 1998. "Economics of product development by users: The impact of "sticky" local information." *Management Science,* **44**, pp. 629–644.

[53] Anderson, N., Mattson, C. A., and Harston, S. P., 2009. "Development of an empirical model for the flow rate of geometric information during reverse engineering." In *ASME International Mechanical Engineering Congress & Exposition November 13-19, Lake Buena Vista, Florida*.

[54] Norton, R. L., 2006. *Machine Design*. Pearson Prentice Hall, Upper Saddle River, NJ.

[55] Adams, B. L., Kalidindi, S. R., and Fullwood, D. T., 2005. *Microstructure Sensitive Design for Performance Optimization*. BYU Academic Publishing, Provo, UT.

[56] Hyer, M. W., 1998. *Stress Analysis of Fiber-Reinforced Composite Materials*. McGraw-Hill, New York, NY.

[57] Daniels, H., 1965. "Ultrasonic welding." *Ultrasonics*, pp. 190–196.

[58] O'Brien, R., 1991. *Welding Handbook*. American Welding Society, Miami, FL.

[59] Ram, G., Yang, Y., George, J., Robinson, C., and Stucker, B., 2006. "Improving linear weld density in ultrasonically consolidated parts." 17th Solid Freeform Fabrication Symposium.

[60] Bhattacharjee, P., Ray, R., and Upadhyaya, A., 2005. "Development of cube texture in pure ni, ni-w and ni-mo alloys prepared by the powder metallurgy route." *Scripta Materialia,* **53**, pp. 1477–1481.

[61] Bunge, H., 1993. *Texture Analysis in Materials Science*. Cuvillier Verlag Gottingen, Gottingen, Germany.

[62] Adams, B. L., Gao, X. C., and Kalidindi, S. R., 2005. "Finite approximations to the second-order properties closure in single phase polycrystals." *Acta Materialia,* **53**, pp. 3563–3577.

[63] Hertzberg, R. W., 1989. *Deformation and Fracture Mechanics of Engineering Materials*. John Wiley & Sons, Inc., New York, NY.

[64] Clement, A., 1982. "Prediction of deformation texture using a physical principle of conservation." *Materials Science and Engineering,* **55**, pp. 203–210.

[65] Taylor, G. I., 1938. "Plastic strain in metals." *Journal of the Institute of Metals,* **62**, pp. 307–324.

[66] Fromm, B., Adams, B., Ahmadi, S., and Knezevic, M., 2008. "Grain size and orientation distribution function of high purity alpha-titanium." In *ICOTOM15: The 15th International Conference on the Textures of Materials*.

[67] Bata, V., and Pereloma, E., 2004. "An alternative physical explanation of the hall-petch relation." *Acta Materialia,,* **52**, pp. 657–665.

[68] Asaro, R., and Needleman, A., 1985. "Texture development and strain hardening in rate independent polycrystals." *Acta Metall Mater,* **33**, pp. 923–955.

[69] Dieter, G. E., 1986. *Mechanical Metallurgy*., 3rd ed. New York, NY. McGraw-Hill, Inc.

[70] Owen, C. B., 2006. "Two dimensional friction stir welding model with experimental validation." Master's thesis, Brigham Young University.

[71] Howell, L. L., 2001. *Compliant Mechanisms*. John Wiley & Sons, Inc., New York, NY.

[72] Todd, B. L., 2008. "A compliant threshold accelerometer sensor integrated with radio frequency identifiable tags." Master's thesis, Brigham Young University.